AS&E

**American Science
and Engineering, Inc.**
955 Massachusetts Avenue
Cambridge, Massachusetts 02139
617-868-1600

MAY 1976

ASE-3935

FINAL REPORT

HIGH RESOLUTION
OZONE MAPPER (HROM)

REPORT PERIOD: APRIL 1975—MAY 1976

CONTRACT NO. NAS5-22326

PREPARED FOR:

NATIONAL AERONAUTICS
AND SPACE ADMINISTRATION
GODDARD SPACE FLIGHT CENTER
GREENBELT, MARYLAND 20771

Final Report

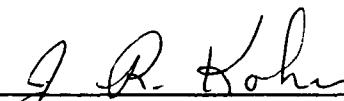HIGH RESOLUTION
OZONE MAPPER (HROM)

Contract No. NAS5-22326

Report Period: April 1975 – May 1976

Prepared by:
American Science and Engineering, Inc.
955 Massachusetts Avenue
Cambridge, Massachusetts   02139

Prepared for:
National Aeronautics and
Space Administration
Goddard Space Flight Center
Greenbelt, Maryland   20771

Approved by:

J. R. Kohr, Program Manager

A. C. Vallas, Vice President

May 1976

1. Report No. NAS-	2. Government Accession No	3. Recipient's Catalog No.
4. Title and Subtitle Design Study for a High Resolution Ozone Mapper		5. Report Date May 1976
		6. Performing Organization Code
7 Author(s) J. Decker (SI), R. Kohr (AS &E), R. Wegant (BI)		8. Performing Organization Report No ASE-3935
9 Performing Organization Name and Address American Science and Engineering, Inc. 955 Massachusetts Avenue Cambridge, Massachusetts, 02139		10 Work Unit No.
		11. Contract or Grant No. NAS5-22326
		13. Type of Report and Period Covered
12. Sponsoring Agency Name and Address Dr. Donald F. Heath, Code 912 Goddard Space Flight Center Greenbelt, Maryland, 20771		Final Report April 1975 – May 1976
		14 Sponsoring Agency Code

15. Supplementary Notes

16 Abstract

This report contains the results of a design study for a High Resolution Ozone Mapper (HROM). Using the present Backscatter Ultraviolet Instrument (BUV) aboard NIMBUS 4 as a baseline, point scanner mechanisms and spatial multiplex scanning systems were compared on the basis of sensitivity, field of view and simplicity. This comparison included both spectral and spatial scanning and multiplexing techniques. The selected system which optimally met the performance requirements for a shuttle based instrument was a "pushbroom" spatial scanner using a 15 element photomultiplier tube array and a Hadamard multiplex spectral scan. The selected system was conceptually designed. This design includes ray traces of the monochromator, mechanical layouts and the electronic block diagram.

17. Key Words (Selected by Author(s)) "Pushbroom" Scanner Hadamard Transform Spectrometer Spectral – Spatial Scanner Shuttle BUV -Imaging Spectrometer	18 Distribution Statement

19. Security Classif. (of this report) Unclassified	20 Security Classif (of this page) Unclassified	21 No of Pages 112	22. Price*

PREFACE

(a)   Objective

The purpose of this study is to achieve a preliminary design for a shuttle based BUV imaging spectrometer that meets the mission requirements.

(b)   Scope of Work

Using the present BUV instrument aboard NIMBUS 4 as a baseline, compare point scanner mechanisms and spatial multiplex scanning systems based on sensitivity, field of view and simplicity. Include in the comparison spatial and spectral scanning and multiplexing techniques, with a view at optimizing the overall system for the basic performance requirements. Select an optimum sensor configuration and perform a conceptual design study for the selected sensor.

(c)   Conclusions

An optimum sensor configuration using a "pushbroom" spatial scanner with a Hadamard spectral scan was selected. This system meets the requirements for a shuttle based mission. A conceptual design was performed on the selected sensor and monochromator ray traces, mechanical layouts and the electronic block diagram were generated.

(d)   Summary of Recommendations

A High Resolution Ozone Mapper should be breadboarded and tested.

TABLE OF CONTENTS

CONTENTS (Continued)

CONTENTS (Continued)

ILLUSTRATIONS

TABLES

1.0   INTRODUCTION

This final report on the High Resolution Ozone Mapper (HROM) is submitted as required under Item 9 of the Statement of Work for Contract NAS5-22326.

The purpose of the study was to achieve a preliminary design for a shuttle based HROM Imaging Spectrometer System that meets the requirements of the subject work statement. This report details the accomplishments of the study.

The performance requirements of the work statement constitute a significant increase in sensitivity over the Backscatter Ultraviolet (BUV) Instrument aboard NIMBUS 4. This instrument was used as a baseline in the study. The BUV instrument for its size and configuration represents a limit in performance for state-of-the art technology. Thus, in order to realize the objective of the study, a different type of approach was required. A more satisfactory approach was realized which combined the obvious advantages of a "pushbroom" scanner using a linear array of detectors for spatial scanning with the improvements derived from using a multiplex system for spectral scanning. This report contains the rationale, analysis and preliminary mechanization design for an instrument which uses this approach and meets the objective of the work statement.

Section 2 of the report discusses the requirements imposed on the instrument to insure faithful reproduction of the ozone profile and radiance level as well as a listing of the overall system requirements.

Section 3 of the report details the results of the candidate sensor tradeoff. In this section, the types of systems initially considered are enumerated. Then, the rationale and analysis by which the number of systems were reduced is detailed. Finally, a candidate tradeoff matrix is generated and the final candidate systems (2) selected.

Section 4 contains the performance evaluation study results. The section briefly discusses the fact that the conventional system can be evaluated by extrapolation from the BUV instrument, but the Hadamard System must be discussed in detail. Thus, the section mainly discusses Hadamard Spectrometers. The sources of noise and the effects of these noise sources on the sensor are delineated. Also, the section discusses errors and their correction. Next, a preliminary design of the Hadamard mask is generated. Finally a comparison of the two candidate sensors is presented, using signal-to-noise ratio as a criteria.

Section 5 contains the selection of the recommended system. The section briefly recounts the rationale used to select the final candidate system.

Section 6 contains the results of the comceptual design activity task. In this section, a preliminary system mechanization is presented. The section contains the mechanical, optical and electronic design for an instrument which meets the requirements for the mission.

This report has been prepared by AS&E, incorporating contributions in the Requirements, Mechanical Design and Optical Design Section from Beckman Instrument, Inc. , and in the Hadamard Multiplexing Section, from Spectral Imaging, Inc.

2.0 EXPERIMENT REQUIREMENTS

The High Resolution Ozone Mapper (HROM) System will provide the ultraviolet sounding and mapping data necessary to calculate and map the changing distribution of the ozone layer surrounding the earth.

To perform these functions, analysis shows that very high spectral resolution must be attained and the stray light reduction and electronic dynamic range must be large.

2.1 Spectral Requirements

The spectral bandpass must be narrow ($\sim 10 \overset{\circ}{A}$), the wavelength accuracy high (± 0.2 to $0.5 \overset{\circ}{A}$) and the dynamic range very large (10^5 to 10^7) because of the steepness of the ozone absorptive edge. The successful performance of the Nimbus 4 BUV for four years in space shows that these requirements can be met reliably.

The extremely rapid wavelength dependence of the earth's ultraviolet albedo at the edge of the strongly absorbing ozone band determines the instrument requirements for spectral bandpass, wavelength repeatability, dynamic range, and stray light.

One can see why the instrument spectral selection requirements need to be as tight as they are by considering the wavelength variation of the received albedo radiance. A plot of received radiance as a function of wavelength is shown in Figure 2-1. This plot is taken from Nimbus 4 BUV data reported by Heath and Heaney. The radiance which would be observed if the solar energy were diffusely reflected from a perfect diffuser with 100% albedo is shown for comparison. The ozone
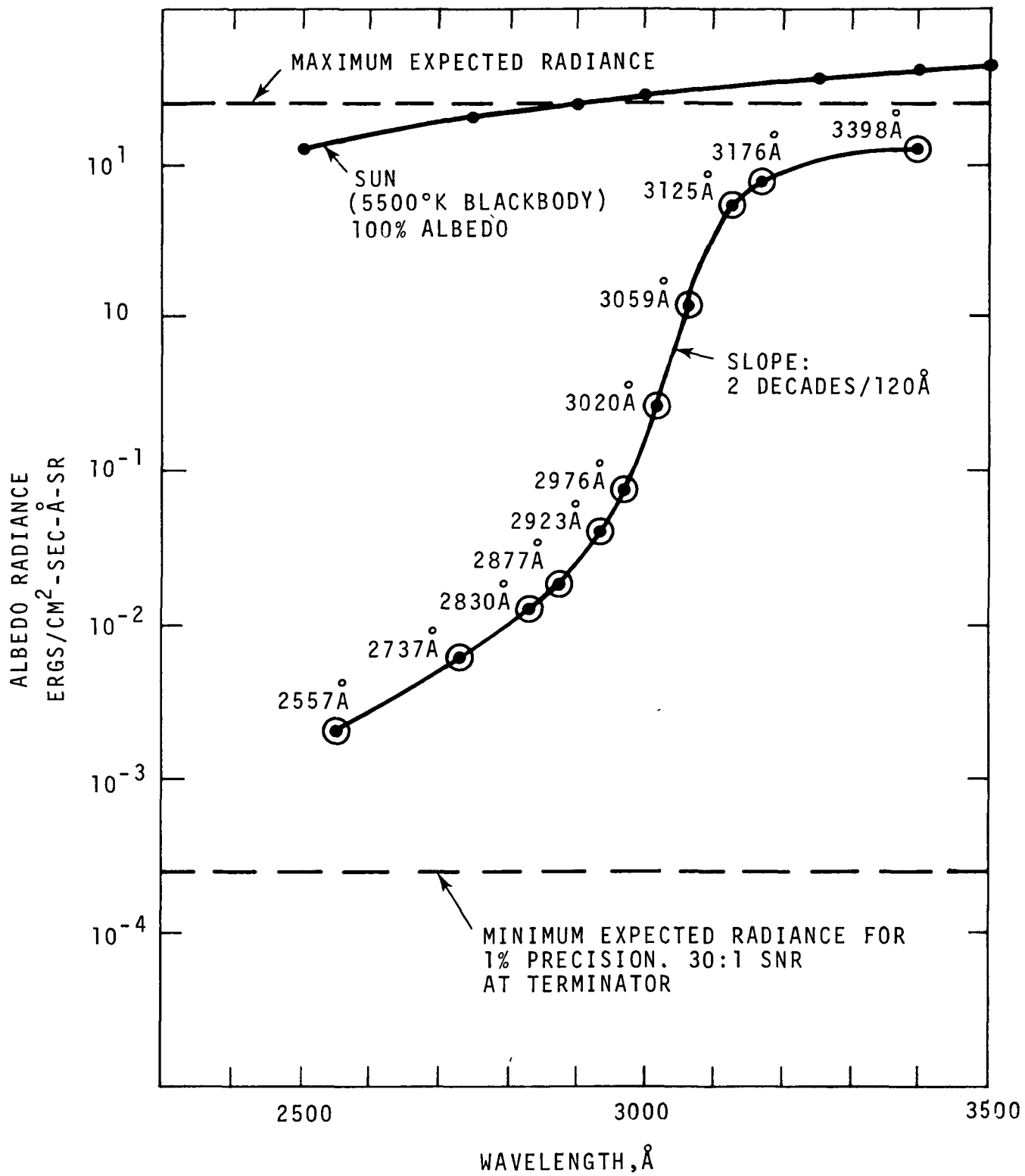
Fig. 2-1 Observed Radiance Versus Wavelength (BUV Orbit 100)

absorption causes a decrease in observed radiance at a rate of 2 decades per 120 $\overset{\circ}{A}$ in the neighborhood of 3050 $\overset{\circ}{A}$.

To infer the ozone profile reliably from the data, the atmospheric albedo must be determined within limits of 1 to 3 percent, which requires measurements of the radiance to 1 percent or better. The bandpass, wavelength accuracy and repeatability of the spectrometer must be so chosen as to contribute only a small part of this error.

2.2   Wavelengtn Accuracy and Repeatability

In the neighborhood of 3050 $\overset{\circ}{A}$ the radiance (N) changes at a rate of two decades over 120 $\overset{\circ}{A}$ (or a factor of e = 2.718 every 26 $\overset{\circ}{A}$.) The fractional error in radiance resulting from a wavelength measurement error $\Delta \lambda$ is then:

$$\frac{\Delta N}{N} = \frac{\Delta \lambda}{\lambda_0} \qquad (2.1)$$

where $\lambda_0 = 26\overset{\circ}{A}$. To obtain an error of $^{+}_{-}1$ percent, the value of $\Delta \lambda$ must be less than 0.26 $\overset{\circ}{A}$.

A slightly reduced value for absolute accuracy of the wavelength can be accepted because several measurements are made but the repeatability of the wavelength to $^{+}_{-}0.2$ to 0.5$\overset{\circ}{A}$ is a necessary requirement.

2.3   Bandpass

If the instrument bandpass is too wide, the profile will be smoothed with loss of information. For a spectrum varying over a limited range, λ_1 to λ the radiance N is given by the expression:

$$N = N \ (\lambda_1) \ e^{(\lambda - \lambda_1)/\lambda_0} . \qquad (2.2)$$

where $N \ (\lambda_1)$ = the radiance at λ_1

The average radiance over a triangular bandpass of width at half-height $\Delta\lambda$ centered at λ_1 is:

$$\overline{N} = 2 \left(\frac{\lambda_0}{\Delta\lambda} \right)^2 \left(\cosh \ \frac{\Delta\lambda}{\lambda_0} - 1 \right) . \qquad (2.3)$$

This average value deviates from $N \ (\lambda_1)$ by an error which, to second order in $\Delta\lambda/\lambda_0$ is given by

$$\frac{\Delta\overline{N}}{N(\lambda_1)} = \frac{1}{12} \left(\frac{\Delta\lambda}{\lambda_0} \right)^2 . \qquad (2.4)$$

For $\Delta\lambda = 10 \overset{o}{A}$, $\lambda_0 = 26 \overset{o}{A}$, the shift in the radiance is 1.2 percent. Although the effect can be corrected by deconvolution, it is desirable to keep it as small as possible. This consideration explains why the spectral bandpass must be as small as 10 $\overset{\smile}{A}$.

2.4   Resolution

The inherent resolution of the instrument must be better than 1 $\overset{o}{A}$ (Rayleigh criterion). If the inherent resolution, which depends on wavelength, were larger, the overall bandpass would exhibit wavelength-dependent variations larger then 1 percent, leading to a comparable error in the spectral radiance.

2.5   Stray Light

Stray light refers to the light of the wrong color detected by the spectrophotometer. (For a filter radiometer, this is conven-

tionally called "out of band response.") Only a double grating monochromator can provide the stray light rejection of 10^6 required to meet the dynamic range requirements.

2.6   System Specification

Table 2.1 contains a list of the system preliminary specifications as contained in the Statement of Work.

TABLE 2.1

PRELIMINARY SPECIFICATIONS

Orbital Altitude   400 Km

Total Field of View $7^\circ \times 104^\circ$

Instantaneous Field of View $7^\circ \times 7^\circ$

Number of Detectors   15

Wavelength of Spectral Bands   2555, 2735, 2830,
                                    2876, 2922, 2975,
                                    3019, 3058, 3125,
                                    3175, 3312,
                                    $3398A^\circ$ (12 Bands)

Band pass (Half Power) $10A^\circ$

Spectral Resolution $1 \, A^\circ$

Stray Light Rejection 10^6

Polarization Sensitivity $< 5\%$

Signal Dynamic Range 10^3

S/N Ratio   30 @ 2.5×10^{-4}
                                    Erg/cm^2 Ster. A°_s

Radiometric Precision   1%

Overlap/Underlap $< 5\%$

3.0   CANDIDATE SYSTEM TRADEOFF ANALYSIS

3.1   Types of Systems Considered

Using the assumption that each detector in a multielement
system must view all the spectral regions (i.e., separate
detectors cannot be used for each spectral region), the
candidate system contained in Table 3-1 were generated. A
description of each of the systems follows:

3.1.1.   Candidate Sensors Which View the Entire 104°
              by 104° Field of View

    a)   Hadamard Spatial and Hadamard Spectral Multi-
              plexing Sensor

              Light from the total field of view is collected by
              the aperture and focused onto a two dimensional
              mask with square open and blocking elements
              (looks like a cross-word puzzle). This mask
              rotates (or steps) at a rate commensurate with the
              frame time (for a 109 sec. frame time each mask
              position must be held for 35 msec). In each
              mask position 255 (15 x 17 elements) of the
              elements are displayed through an area determined
              by a rectangular field mask. One hundred twenty
              eight (128) of these elements pass light, and one
              hundred twenty seven (127) elements block it in
              any given mask position. There are two hundred
              fifty-five (255) independent positions for this mask.
              The mask contains a total of 957 elements for
              each frame scanned.

TABLE 3-1

TYPE OF SYSTEMS CONSIDERED

	Spatial	Spectral
1. View Entire 104° FOV	a. 2 Dim H	1 Dim H
	b. Image Plane Scanner	1 Dim H
	c. Image Plane Scanner	C
	d. Image Tube	Undecided
	e. Mosaic Array	Undecided
2. View FOV of 104° by $7X^\circ$	a. 1 Dim H	1 Dim H
	b. Image Plane Scanner	1 Dim H
	c. Image Plane Scanner	C
	d. Image Tube	Undecided
	e. Mosaic Array	Undecided
3. View Hor. Line 104° Wide by 7° High	a. 1 Dim H	1 Dim H
	b. 1 Dim H	C
	c. 15 element lin array	1 Dim H
	d. 15 element lin array	C
4. View Vert. Line 104° High by 7° High	a. 1 Dim H + OPS	1 Dim H
	b. 1 Dim H + OPS	C
	c. Linear Array + OPS	1 Dim H
	d. Linear Array + OPS	C
5. View One Spatial Res Elm 7° by 7°	a. OPS	1 Dim H
	b. OPS	C
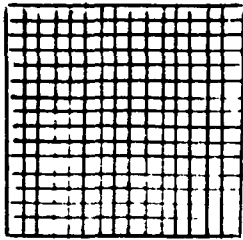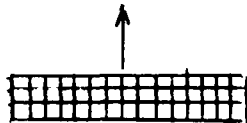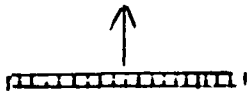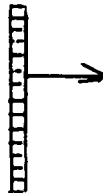
Where

2 Dim H   Two dimension Hadamard Mask

1 Dim H   One dimension Hadamard Mask

C   Same Spectral Scanning as BUV

OPS   Object Plane Scanner

After passage through the mask the modulated radiation
is dispersed by the monochromator and refocused onto
a second mask. This second modulating mask is a one
dimensional spectral mask. It consists of 23 slits, some
open, some opaque. Twelve of these slits are exposed
at one time. There are also twelve independent positions
for this mask. Each position must be held for a full cycle
of the first mask (approximately 9 sec.). After passing
through the second mask the spatial and spectral encoded
radiation is de-dispersed and focused onto a PMT.

The electrical output of the PMT is conditioned and con-
verted to digital format. The digital words are then
telemetered to the ground station, where the Hadamard
transform is performed on the data to reconstruct the
scene.

b) Image Plane Scanner Spatial Scan With A Hadamard
Spectral Scan

An image of the entire 104° square field is produced using
a lens system and an image plane scanner is used to
interrogate this field pixel by pixel. A modified BUV
monochromator is employed with a single phototube and
a Hadamard one dimensional spectral mask scans the
wavelengths.

Several image plane scanner types could be used, but in
a system with an aperture less than approximately 8 inches
there is no advantage in mechanical complexity over an
object plane scanner. The simpler types of image plane
scanners counter rotating wedges, reticles would require
a form of image motion compensation to direct the light

3 - 3

through the monochromator. The more complex image plane scanners such as the squirrel cage or the roof mirror are significantly more complex than an object plane scanner such as that used in TOMS and would be difficult to build in the small size required by HROM. External reflecting polygons and two axis oscillating mirrors are about equal in complexity to the TOMS scanner and would have the same system throughput.

The radiation from each pixel in the image plane is dispersed by the monochromator and focused onto a Hadamard one dimensional mask containing 23 slits. Twelve slits are exposed at one time and there are twelve independent positions. Each position must be held for one complete scan of the image plane (one field) approximately 9 sec. After passing through the mask the modulated radiation is de-dispersed and focused onto a PMT.

The electrical output from the PMT is conditioned digitized, telemetered and Hadamard transformed to reconstruct the original scene.

c)   Image Plane Scanner Spatial Scan With Conventional Monochromator

This system is the same as (b) above except for spectral scanning. The present BUV monochromator is employed with a single phototube and a step scan through the wavelengths.

d)   Image Tube Systems

Ultraviolet image tubes are available with sensitivity adequate to meet this specification. One such tube is the Digicon, wherein photoelectrons from an end-on semi-transparent photocathode are accelerated and magnetically focused on an array of silicon diodes. Tubes of this type with 1024 elements have been built.

While it is not clear how the spectral requirements could be met, the extreme sensitivity of these devices makes the approach interesting.

A system built recently at the University of Texas was capable of counting as few as one photoelectron every four minutes. Unfortunately, saturation of these devices occurs at a total count of about 6000 photoelectrons. To accommodate the dynamic range of HROM the system integration time would have to change with signal level by about three orders of magnitude. While circuitry could be designed for this, the low saturation level corresponds to a limitation on measurement accuracy of about 2%. Another source of error arises from the fact that the diode array is also sensitive to light from 4000 to 10,000 $\overset{o}{A}$. In the University of Texas system, which was operating at approximately 4000 $\overset{o}{A}$, the error from a Tungston source was 2%. For HROM it would probably be much larger. Two additional problems, radiometric nonlinearity and the necessity for refrigeration to approximately $-80^{\circ}C$ reduce the attractiveness of this system in spite of its sensitivity.

e)   Mosaic Arrays

Mosaic arrays are available with sensitivity adequate
to meet this specification. The arrays are presently
silicon detectors with CCD or CID readouts. Arrays
of this type have been produced with up to 1024
elements.

The major drawback to this type of system is in the
dynamic range. Present devices only operate over
two to three orders of magnitude. The major problem
area is saturation in the CCD device. Thus while
mosaic arrays are attractive from a system mechaniza-
tion standpoint, the devices are not sufficiently de-
veloped for this application.

3. 1. 2.   Candidate Sensors which View A Portion of the Total
            Field of View

a)   Hadamard Spatial and Hadamard Spectral Multi-
        plexing Sensor

This sensor is similar to sensor 1a, the only difference
is the two dimensional spatial mask, which in this
case is 15 elements wide by x elements high (depend-
ding on the vertical field of view).

b)   Image Plane Scanner For Spatial Scan With a Hadamard
        Spectral Scan

It is possible to construct an imaging system which
would view a total field of 104° in one dimension
and less than 104° in the other dimension. Both
systems 1c) and 1d) above could be configured in
this manner but there is no obvious advantage other
than minimizing the effects of sun angle changing

3 - 6

during the period of measurement. The system

mechanization considerations are the same.

c)   Image Plane Scanner For Spatial Scan With A
Conventional Monochrometer

See Section   3. 1. 1. c.

d)   Image Tubes

This system is similar to system 1d. It is possible

to construct an imaging system which only views

a portion of the field. However, there is no obvious

advantage to this system.

e)   Mosaic Array

This sensor is similar to sensor ie., the only difference

is in the number of detectors in the array.

3. 1. 3.   <u>Pushbroom System</u> (View a line 104° wide by 7° high)

a)   Hadamard Spatial and Hadamard Spectral Multiplexing
Sensor

The light is collected by the aperture slit and dis-

persed perpendicular to the 104° direction by the

monochromator and focused onto a two dimensional

Hadamard mask. The mask encodes the spatial informa-

tion in the direction parallel to the 104° and spec-

trally in the direction of dispersion. The mask will expose

15 x 12 elements for each position and have 15 positions.

Possibly the mask will be on a wheel with 12 one dimen-

sional 15 element separate masks which rotate into

place. The energy passing through the mask will be

de-dispersed and focused onto a single PMT.

b)   Hadamard Spatial and Conventional Spectral Sensor

The light is collected by the aperture and focused
onto a one dimensional Hadamard mask containing
29 slits. The mask exposes 15 slits at any one time
and has 15 independent positions. The encoded
radiation passing through the mask is dispersed by a
monochromator and focused on an exit slit. The mono-
chromator is a modified BUV design with a single
phototube and a step scan through the wavelengths.

c)   Linear Array Spatial Scan with a Hadamard Spectral
        Scan

A lens is used to image a field 104° wide and 7° high.
A linear array of 15 photomultipliers detects the energy
in the 15 pixel wide field. Since system sensitivity
increases with the square root of the number of detec-
tors, an improvement in signal-to-noise ratio of four-
fold is achieved. The monochromator is a modified BUV
design where the dispersed radiation is focused onto
a one dimensional Hadamard mask containing 29 slits.
Twelve of the transmissive and opaque slits are ex-
posed to the radiation for a time comenserate with
the frame time. There are 12 independent mask positions.
The encoded radiation passing through the mask is
de-dispersed and focused onto the linear array of 15 PMT's.
The linear array does the spatial scanning.

d)   Linear Array Spatial Scan with a Conventional Mono-
        chromator

This system is the same as 3c except the present BUV
monochromator concept is used to provide the spectral

information and the only modification is a rotation
of the monochromator so that dispersion is in the
direction of the flight vector. The system is basically
the same as the present BUV except for the imaging
lens and the increased number of detectors and pre-
amplifiers.

It would also be possible to configure the system so that
the extra detectors are used in the spectral domain. The
matching of the photomultipliers would then become
a major instrument design problem. Gain stability,
linearity over the total dynamic range and space radi-
ation effects could lead to errors unable to be removed by
calibration. For this reason no systems were considered
wherein multiple detectors were used for the different
ozone absorption wavelengths.

3.1.4.   Object Plane Scanning Systems (Views a Field of View
          104° high by 7° wide)

An object plane scanner could be employed with an
array of detectors. The system sensitivity would
be improved by the square root of the number of detec-
tors used. The system telescope requires an imaging
lens in addition to the mechanical scanner. If 15
detectors are used there would be no advantage to these
systems over the pushbroom scanners described above
and they would have the additional complexity of the
added scanning mechanism. If less than 15 detectors
are used, the sensitivity improvement would be diminished.
One advantage of an object plane scanner over a push-
broom is that they are somewhat easier to calibrate. The

3 - 9

calibration can be done during the dark period of the scan cycle. With a pushbroom, the calibration sequence results in loss of ground coverage for the duration of the sequence.

3.1.5.   <u>Point Scanning System</u> (View a Field of View 7° by 7°)

An object plane scanner could be employed with a single detector. The scan is perpendicular to the flight vector. The system telescope requires a narrow field of view lens (7°) in addition to the mechanical scanner. For system 5a a Hadamard mask, which is the same as that used in system 3c, is used for spectral scanning. In system 5b, a BUV monochromator with a stepping through the wavelengths is used. This type of system is very similar to the present BUV and the sensitivity does not meet the requirements.

3.2   First Reduction of Candidate Systems

Referring to Table 3-1 several systems were eliminated by inspection. These included:

1.   Image Plane Scanning Systems (Systems 1b,1c, 2b and 2c). Since the aperture diameter for the HROM system is small, an image plane scanner has no size advantage over an object plan scanner. Also the image plane scanner requires wide angle optics. Therefore, it was decided to eliminate these systems.

2.   System Ulilizing Image Tubes (Systems 1d and 2d) Since image tubes do not have the capability to meet the dynamic range   requirements, these systems were also eliminated from further consideration.

3.   Systems Employing Mosaic Arrays (System 1e and 2e) Mosaic arrays of detectors with CCD readout were considered. However, state-of-the-art devices only have a 10^4 dynamic range capability. Thus, these systems were eliminated.

In this manner, the number of candidate sensors to be analyzed was reduced to 12 systems.

3.3   Signal-To-Noise Ratio Evaluation

In order to further reduce the number of candidate systems, the systems were compared on a basis of signal-to-noise ratio.

Equations were derived for the signal-to-noise ratio for both conventional and Hadamard scanning systems and these equations were used to calculate the SNR for each of the twelve systems.

3.3.1   Conventional System (point scanning system)

For a photomultiplier system:

$$\frac{S}{N} = \frac{N_s}{\Delta f^{1/2} \left[N_s + N_D \right]^{1/2}} \qquad (3.1)$$

where:

N_s = Number of photoelectrons per second from the source

Δf = System bandwidth

N_D = The sum of the number of photoelectrons per second from the detector dark current, the trapped electron, X-rays and protons.

3.3.2   Hadamard Multiplex System

For a Hadamard sensor, since more than one spatial element is viewed simultaneously, equation (3.1) becomes:

$$\left(\frac{S}{N}\right)_H = \frac{N_s \left(\frac{M \times P}{2N}\right)}{\Delta f^{1/2} \left[N_s \frac{M \times P}{2N} + N_D \right]^{1/2}} \qquad (3.2)$$

where:

     M = Number of spatial elements scanned (Pixels)

     P = Number of spectral elements

     N = Number of masks required (transmission factor)

however:

$$\left(\frac{S}{N}\right)_H \quad \text{is only the ratio for 1 field (one look)}$$

For the S/N ratio for a single pixel in the field

$$\left(\frac{S}{N}\right)_{H'} = \left(\frac{S}{N}\right)_H \times (M \times P)^{-1} \tag{3.3}$$

But in a full frame each pixel is viewed (M x N) times and since the S/N ratio improves by the square root of the number of looks

$$\left(\frac{S}{N}\right)_{H''} = \left(\frac{S}{N}\right)_{H'} \times (M \times P)^{1/2} \tag{3.4}$$

substituting eq. (3.3) into eq. (3.4):

$$\left(\frac{S}{N}\right)_{H''} = \frac{\left(\frac{S}{N}\right)_H}{(M \times P)} \times (M \times P)^{1/2}$$

$$\left(\frac{S}{N}\right)_{H''} = \left(\frac{S}{N}\right)_H \times (M \times P)^{-1/2} \tag{3.5}$$

substituting eq. (3.2) into eq. (3.5):

$$\left(\frac{S}{N}\right)_{H''} = \frac{N_s \left(\frac{M \times P}{2N}\right)}{\Delta f^{1/2} \left[N_s \left(\frac{M \times P}{2N}\right) + N_D\right]^{1/2} (M \times P)^{1/2}} \tag{3.6}$$

simplifying eq. (3.6)

$$\left(\frac{S}{N}\right)_{H''} = \frac{N_S \ (M \times P)^{1/2}}{2N\Delta f^{1/2} \left[N_S \left(\frac{M \times P}{2N}\right) + N_D\right]^{1/2}} \qquad (3.7)$$

For noise in signal limited operation equation (3.7) becomes:

$$\left(\frac{S}{N}\right)_{H''} = \frac{N_S^{1/2}}{(2N\Delta f)^{1/2}} \qquad \left(N_S \gg N_D\right) \qquad (3.8)$$

For additive noise limited operation eq. (3.7) becomes:

$$\left(\frac{S}{N}\right)_{H''} = \frac{N_S \ (M \times P)^{1/2}}{2N \ \Delta f^{1/2} \ N_D^{1/2}} \qquad \left(N_D \gg N_S\right) \qquad (3.9)$$

3.3.3   Additive Noise (N_D)

Figure 3-1 shows the S/N ratio for the twelve candidate systems. For this analysis the value of N_D was set at 2×10^3 photo electrons per second for a minimum value and 1.95×10^7 photo electrons per second for the maximum value. The curves were generated using equations (3.1) and (3.7) where the values for the parameters are contained in Table 3.2. The minimum value of additive noise (N_D) was obtained from the "quiet" values obtained from the BUV flight. The maximum value of additive was obtained from calculation at 400 Km in the South Atlantic Anomaly.
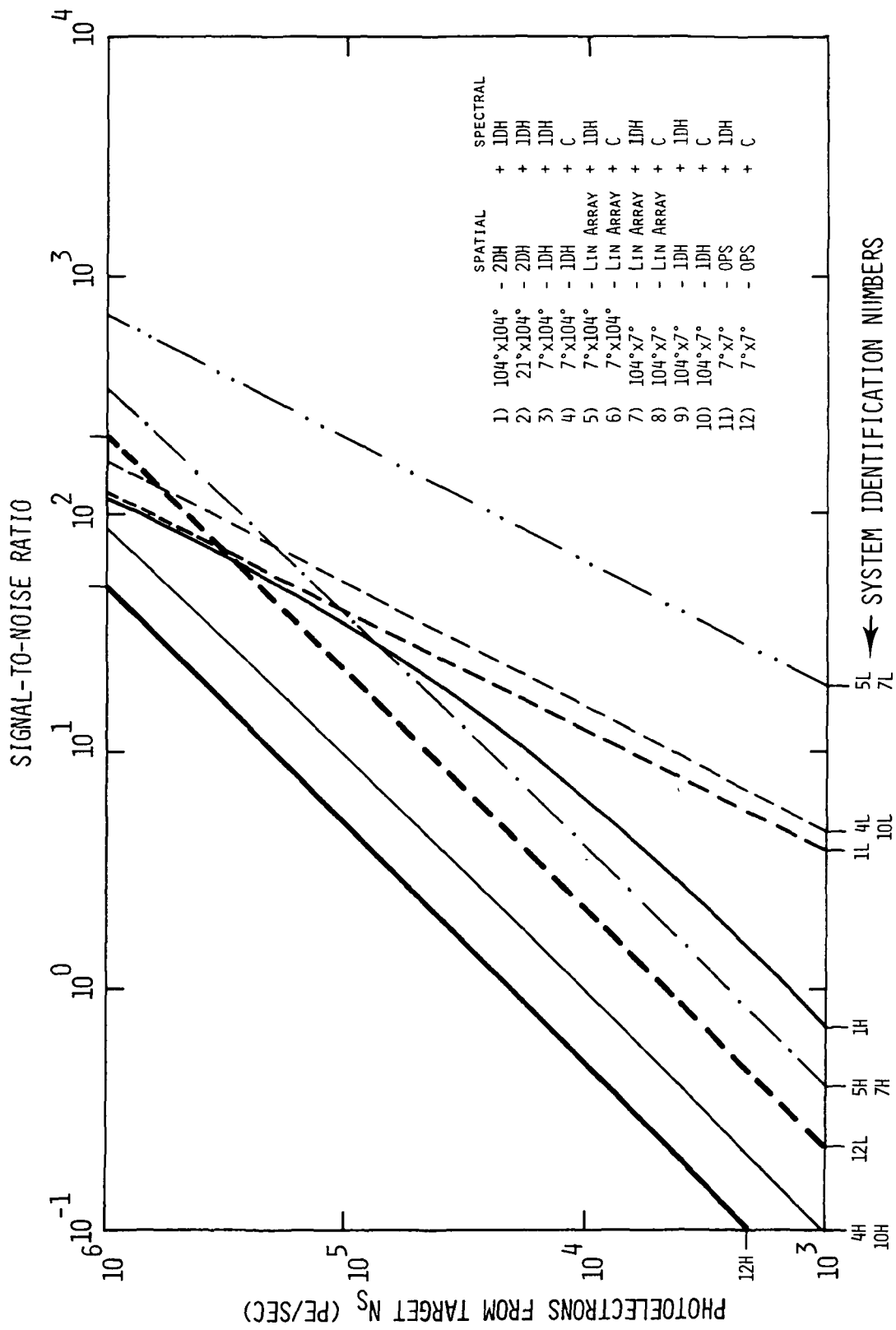
Figure 3-1. Signal-to-Noise Ratio vs Number of Photoelectrons From The Target For A Detector Noise Level of 2×10^3 pe/sec (L) and 1.95×10^7 pe/sec (H).
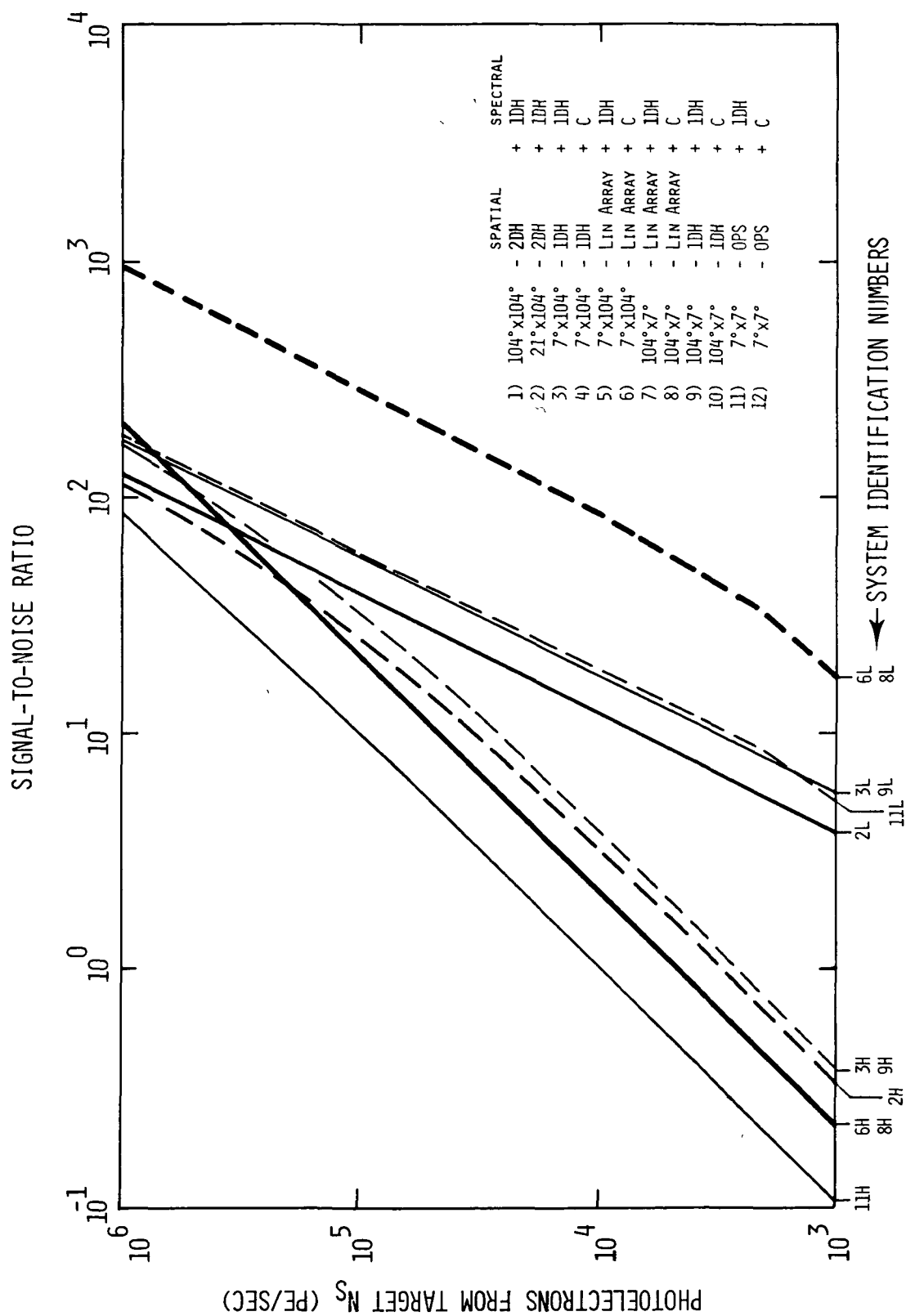
Figure 3-1 (Continued)

System #	Table 3.1 Designation	Equation # Used	N_s Pe/sec	M	P	N	N_d Pe/sec	Δf Hz
1	1a	3.7	Variable	225	12	2	1.95×10^7 (high) 2×10^3 (Low)	16.5
2	2a	3.7	Variable	45	12	2	1.95×10^7 (High) 2×10^3 (Low)	16.4
3	3a	3.7	Variable	15	12	1	1.95×10^7 (High) 2×10^3 (Low)	15.4
4	3b	3.7	Variable	15	1	1	1.95×10^7 (High) 2×10^3 (Low)	19.3
5	3c	3.7	Variable	1	12	1	1.95×10^7 (High) 2×10^3 (Low)	1.03
6	3d	3.1	Variable	-	-	-	1.95×10^7 (High) 2×10^3 (Low)	1.1

Table 3.2

Values Used in S/N Equations

System #	Table 3.1 Designation	Equation # Used	N_s Pe/sec	M	P	N	N_d Pe/sec	Δf Hz
7	4c	3.7	Variable	1	12	1	1.95×10^7 (High) / 2×10^3 (Low)	1.03
8	4d	3.1	Variable	-	-	-	1.95×10^3 (High) / 2×10^3 (Low)	1.1
9	4a	3.7	Variable	15	12	1	1.95×10^7 (High) / 2×10^3 (Low)	15.4
10	4b	3.7	Variable	15	1	1	1.95×10^7 (High) / 2×10^3 (Low)	19.3
11	5a	3.7	Variable	1	12	1	1.95×10^7 (High) / 2×10^3 (Low)	15
12	5b	3.1	Variable	-	-	-	1.95×10^7 (High) / 2×10^3 (Low)	19.3

Table 3.2 (Cont'd)

The bandwidth terms were obtained using the following equations:

$$\Delta f = \frac{A_x A_y A_\lambda T_f}{2 n_d K} \qquad (3.10)$$

where A_x = Number of pixels in x direction

A_y = Number of pixels in y direction

A_λ = Number of spectral regions

T_f = Frame time (1/sec)

n_d = Number of detectors

K = Scan efficiency

Notice in Figure 3-1 that under low background conditions the systems are essentially signal noise limited and the point scanning systems have the better S/N. However, under high background conditions the multiplex systems are superior.

3.3.4   Source Photoelectron Value Set Constant

Figure 3-2 is a replot of Figure 3-1 where N_s is held constant at a nominal value and N_D varies. All the other values in the equations are the same as in Table 3-2. From these curves it is obvious that the type of system to be selected is heavily weighted by the expected background (N_D term).

3.4   Candidate System Trade Off Matrix

A tradeoff matrix for the twelve candidate system is shown in Table 3.3. An explanation of the table heading follows:

a.   S/N - This column shows the calculated S/N ratio for each system for a constant target flux (N_s) of 5×10^4 pe/sec and a low background level (N_D) of 2×10^3 pe/sec on top and a high background level (N_D) of 1.95×10^7 pe/sec below.
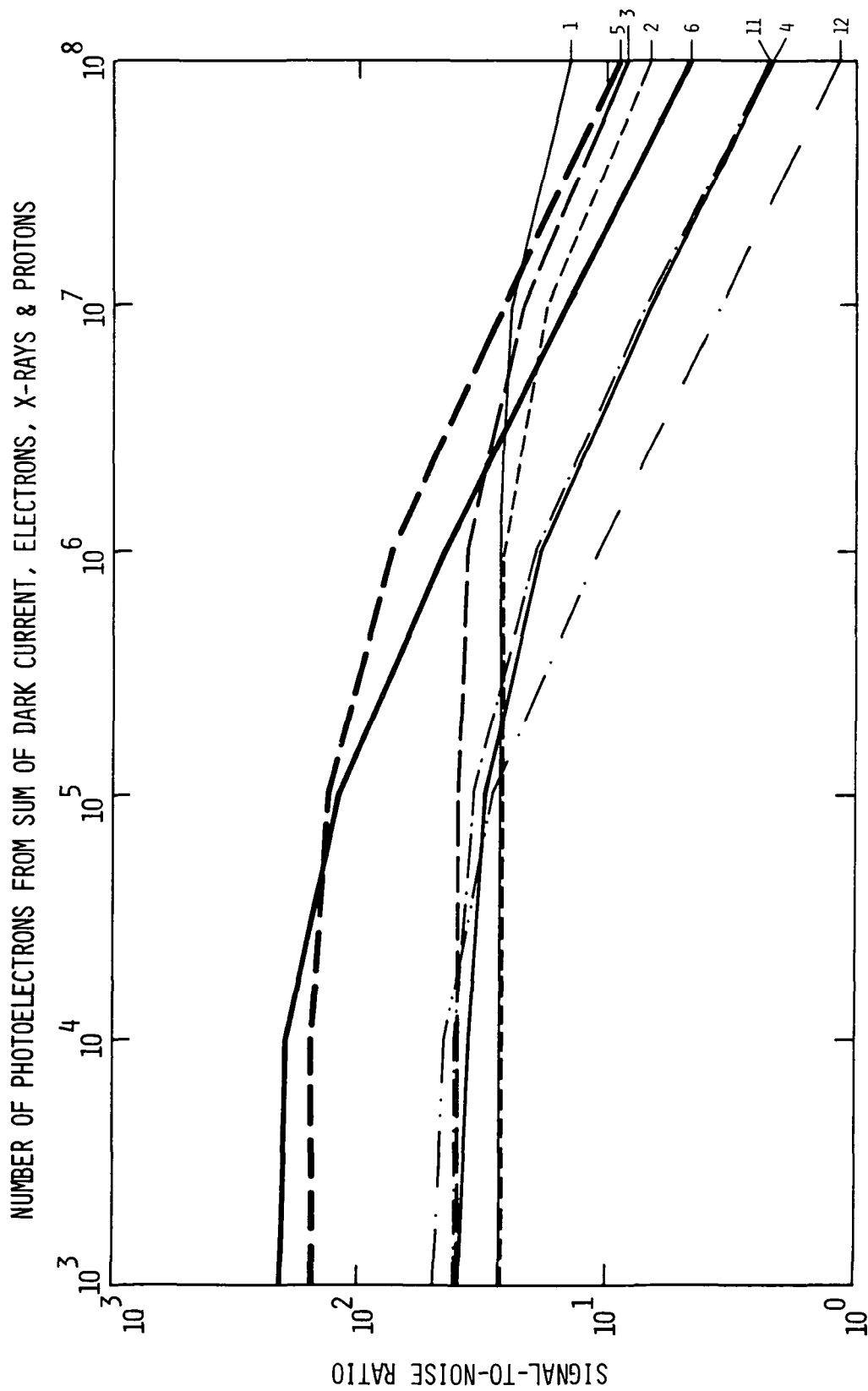
3 - 19

Figure 3-2. Signal-to-Noise Ratio vs Number of Photoelectrons From Additive Noise (N_D) For A Constant Value of Signal Photoelectrons (N_S) of 5×10^4 Photoelectrons/sec.

NUMBER OF PHOTOELECTRONS FROM SUM OF DARK CURRENT, ELECTRONS, X-RAYS & PROTONS

SIGNAL-TO-NOISE RATIO

3-20

Candidate Systems (Spatial)	(Spectral)	S/N $N_S = 5 \times 10^4$ Pe/Sec	S/N Improvement	Number of Detectors	Field of View	Dwell Time/FOV sec	Bandwidth Hz	Space Radiation	Optical System Field of View	Image Motion Compensation	Sun Angle	Statistical Independence	Stray Light	Number of Multiplex Masks	Comments
1 2 Dim H	1 dim H	27 5 / 21 9	56 / 8.6	1	104° x 104°	109	16 5	1 00	Wide Angle 2 Dim	Y	N	N	U	2 25%	Wide entrance slits – cause a spectal image overlap – cannot look at only 12 spectral bands
2 2 Dim H	1 dim H	27 6 / 14 0	81 / 5 5	1	21° x 104°	22	16 4	1 56	Wide Angle 1 Dim	Y	N	N	U	2 25%	Mask cannot be designed
3 1 dim H	1 dim H	40 3 / 17 4	81 / 6 8	1	7° x 104°	7 3	15 4	1 84	Wide Angle 1 Dim	Y	N	N	U	1 50%	
4 1 dim H	C	35 9 / 4 9	72 / 1 9	1	7° x 104°	7 3	19 3	5 78	Wide Angle 1 Dim	Y	N	N	U	1 50%	
5 Lin Array	1 dim H	155 3 / 19 2	3 1 / 7 5	15	7° x 140°	7 3	1 03	6 45	Wide Angle 1 Dim	N	N	N	U	1 50%	
6 Lin Array	C	209 4 / 10 8	4.2	15	7° x 104°	7 3	1 096	15 44	Wide Angle 1 Dim	N	N	N	N	0 100%	Most Sensitive System
7 Lin Array-OPS	1 dim H	155.3 / 19.2	3 1 / 7.5	2 to 15	7° x 7°	1 to 7 3	1 03	6 45	Wide Angle 1 Dim	N	N	N	U	1 50%	
8 Lin Array-OPS	C	209 4 / 10.8	4 2	2 to 15	7° to 7°	1 to 7 3	1 096	15 44	Wide Angle 1 Dim	N	N	N	N	0 100%	
9 1 dim H-OPS	1 dim H	40.3 / 17 4	81 / 6.8	1	104° by 7°	7 3	15 4	1 84	Wide Angle 1 Dim	N	N	N	U	1 50%	
10. 1 dim H-OPS	C	35.9 / 4 9	72 / 1.9	1	104° by 7°	7 3	19.3	5 78	Wide Angle 1 Dim	N	N	N	N	1 50%	
11. OPS	1 dim H	40 6 / 5 0	82 / 2 0	1	7° by 7°	0 5	15	6 45	No Wide Angle	N	N	N	U	1 50%	
12 OPS Present BUV	C	49 5 / 2 5	1	1	7° by 7°	5	19.3	12.68	No Wide Angle	N	N	N	N	0 100%	Present BUV

HROM CANDIDATE SYSTEMS

Table 3-3

b. S/N improvement – setting system number 12 (the present BUV instrument) at 1, a calculation was performed to show the improvements achieved in the other system. The number in the top is for a low background and the number in the bottom is for a high background.

c. Number of detectors – This column contains the number of detectors used in each system.

d. Field of view – This parameter is the total field of view that the system images without scanning.

e. Dwell Time/FOV – The time allowed for one field of view.

f. Bandwidth – The system bandwidth.

g. Space Radiation – This parameter is a calculated weighting factor derived from the S/N ratio under high background conditions. The factor is normalized to the Number 1 system. Increases in the value mean that the system is degraded by background.

h. Optical System Field of View – This parameter implies the complexity of the objective lens.

i. Image Motion Compensation – Does the system require image motion compensation? Since the vehicle is moving does the scene move during a frame. Y is yes and N is no.

j. Sun Angle – Is the system effected by sun angle? Y is yes, N is no.

k. Statistical Independence – Is each sample statistically independent? ie. Does the MTF have a quasi square roll off or a 3db per octive roll off? Y is yes, N is no.

l.   Stray Light - Can the stray light be controlled in the
        system - U is unknown, N is no.

m.   Number of Multiplexing Masks - The number of masks
        required and the % transmission of the masks is contained
        in this column.

n.   Comments - Pertinent comments on the system.

From Table 3. 3 the following reduction in candidate systems
have been performed:

a.   Systems 1 and 2 can be eliminated since system 1
        has a problem with the monochromator (see comments)
        and the dwell time is too long. System 2 is eliminated
        because the mask probably cannot be made. This
        system may also have monochromator problems as
        in system 1.

b.   System 4 is eliminated because the S/N improve-
        ment is not adequate.

c.   Systems 7, 8, 9, and 10 are eliminated because they
        are essentially the same as systems 3, 4, 5, and 6,
        besides which they require an object plane scanner.

d.   Systems 11 and 12 are eliminated because the S/N
        improvements are not adequate.

Thus we are left with systems 3, 5 and 6. If the background is
high (2×10^7 pe/sec) then system 3 is a viable solution. How-
ever, since the predicated mission does not have backgrounds in
this region, system 3 was also eliminated.

3. 5   Final Candidate Systems

By process of elimination the selection of only two systems for
further analysis was made. The two systems are systems 5
and 6. Both of these systems perform the spatial scanning
with a 15 element photomultiplier tube array in the direction
perpendicular to the flight path and by the forward motion of
the vehicle in the direction of flight. This type of system is
called a pushbroom scanner. In the spectral domain the
scanning is accomplished by either a Hadamard mask or in the
same manner as the present BUV system.

4. 0   PERFORMANCE EVALUATION

4. 1   General

The two candidate systems selected in the candidate tradeoff
analysis (Section 3. 0) are a pushbroom spatial scanner using
either convention or Hadamard spectral scanning. For the
conventional spectral scanning system, the performance has
been based on an extrapolation of the BUV sensor, and, therefore,
does not have to be proven. On the other hand, the Hadamard
spectral scanning has inadequate performance history and thus
theoretical and experimental results are presented to help
characterize performance. Since the spatial scanning uses the
pushbroom technique, which is well understood, only the
Hadamard Multiplex Spectrometer will be discussed.

4. 2   Hadamard Multiplex Spectrometer

4. 2. 1   General Description

A multiplex spectrometer is sensitive to many of the total
number of individual wavelengths in the spectrum simultaneously.
In comparison, a conventional scanning spectrometer (like the
BUV) is only sensitive to a single wavelength at any one time.
Thus, the multiplex spectrometer is more efficient. Mechanically,
the single exit slit of a conventional spectrometer is replaced
by a multislit mask which allows more light to pass through the
spectrometer to the detector.

Also, Hadamard spectrometers are transform spectrometers,
since the raw data stream from the instrument is a mathematical
transform of the optical input spectrum. Hence, they share with
Fourier-transform spectrometers the requirement for postmeasure-
ment decoding by a digital computer to recover the optical
spectrum. The theory of operation of Hadamard-transform

spectrometers is covered in Appendix A.   If one expresses the basic measurement operation in matrix notation, several things become apparent.   First, that the multiplexing operation is essentially one of optically "writing a set of simultaneous linear equations in the n unknown spectral power densities" (that is, the unknown power of each of the n discretely resolved wavelengths in the spectrum).   Next, that the "coefficient matrix" of this set of simultaneous equations simply describes whether a given wavelength is transmitted or blocked for any given measurement.   Hence, the coefficient matrix is binary, corresponding to the two possible transmission states (say "1" for a transmitted wavelength and "o" for a blocked wavelength). The mathematical requirement for a solution to this set of equations to exist is that the coefficient matrix be "orthogonal", hence we are dealing with "binary orthogonal matrices".   By definition, these are "Hadamard matrices." (the name for any binary orthogonal matrix), or are derived from them, hence the name of the technique.

The codes based on the Hadamard matrix can be demonstrated to be optimum when a single Hadamard mask is used for spectral multiplexing.   (The Fourier transform, for instance, is theoretically a factor of two worse than the cyclic Hadamard-core "S-code" commonly used for HTS spectrometry (Tai and Harwit, 1976).

It should be pointed out that the Hadamard transform is a spatial transform, not a frequency or time-domain transform.   Essentially, the Hadamard transform multiplexes a brightness distribution in space (the spectrum dispersed at the exit focal plane of the "disperser"), and assumes that the brightness distribution is

constant with time. As such, it is more analogus to a photographic plate than to a time-resolved photomultiplier tube.

4.3   Sources of Noise: Effect on Transform Spectrometers

Multiplex spectrometry should only be used if the resulting spectrum has an improved signal-to-noise ratio (SNR), or if greater spectral coverage or resolving power can be attained. If such advantages do not accrue, multiplex techniques generally imply increased expense and should be avoided.

The discussion of SNR advantages is complex, because many different factors can contribute to the noise of a spectrum.

In this section we will list some of the sources of noise and show how they scale. This should give a reasonably clearcut view of the conditions which make spectromodulation desirable and those which do not.

4.3.1   Sources of Noise

A. Photon Noise

The radiation incident on a detector can be considered to consist of photons arriving randomly distributed in time. Strictly speaking, this complete randomness is true only of coherent radiation at low intersity levels, but for most purposes, that restriction is not important. If N_1 photons interact with a detector in a given time interval, the random signal fluctuations will be of order $N_1^{1/2}$, and the ratio of the signal to photon noise is $\sim N_1 / N_1^{1/2} = N_1^{1/2}$,

$$N_p \sim N_1^{1/2} .$$ (4.1)

B. Background Noise

If the detector sees a considerable background signal, a further contribution to the noise can result. If the background - say thermal emission from the detector housing, or from the spectrometer - is unmodulated, it merely adds on to the photon noise due to the radiation whose spectrum is to be analyzed. If the radiation again provides N_1 photons in a time interval, and the background produces N_2 photons which interact with the detector, the total noise will be

$$N_B \sim (N_2 + N_1)^{1/2}. \qquad (4.2)$$

The background noise however need not always be uniform. A distant source whose spectrum is analyzed through a changing atmosphere may produce detector readings which reflect time-varying atmospheric emission.

The atmospheric noise N_{atm} then has a form

$$N_{atm} \sim a(t) N_2. \qquad (4.3)$$

where $a(t)$ is an effective variability in the atmospheric emissivity. Its absolute value ranges from 0 to 1. Its effects on the readings can strongly depend on the modulation employed in obtaining readings, since variations in atmospheric emissivity have peaks at certain modulation frequencies. Unfortunately, such variations appear to be wavelength dependent, and not enough is known about this type of noise to guide, say an astronomer wishing to make infrared observations at the most effective modulation frequency.

C. Modulation or Scintillation Noise

A source of noise similar to that given by Eq. (4.3) is the unintended modulation the incident beam undergoes on its way to the detector. Sources of this noise may be atmospheric scintillation, or atmospheric patchiness - variable cloud cover, for example. Effectively the noise then has a character

$$N_{md} \sim \beta(1)N_1. \qquad (4.4)$$

and again the various Fourier components of the time varying function $\beta(t)$ generally are not known.

D. Detector Noise

Many detectors have intrinsic noise levels much higher than the photon noise. This noise often is modulation frequency dependent and the experimenter normally elects to make his measurements in a frequency interval in which the noise is low. Once this has been done, the rms noise integrated over an observing time T is proportional to $T^{1/2}$. If the noise in unit time interval is n_1:

$$N_d \sim n_1 T^{1/2}. \qquad (4.5)$$

For some types of detector, the noise is also proportional to the square root of the detector area A. For these detectors

$$N_A \sim n_2 T^{1/2} A^{1/2}. \qquad (4.6)$$

where n_2 is the noise per unit detector area.

Other detectors effectively have high noise at high modulation
frequency. This comes about because some very low noise
detectors have very high impedance, and a detector's
response time constant may become so long that neither the
signal nor the noise is properly registered in available
measuring time intervals. In such a situation, amplifier
noise will become smaller at higher modulating frequencies.
As the observing time decreases, the noise effectively goes
up, if the signal is maintained constant by increasing the gain:

$$N_{amp} \sim T^{-1/2}. \qquad\qquad (4.7)$$

E. Minimum Detector Size

Sometimes the minimum available detector size is much
larger than the finest resolution element of available masks.
To make optimum use of the sensitive detector area, encoding
may then be indicated. For minimum available detector size,
this noise N_{size} scales like N_d or N_{amp}, Eqs. (4.5) and (4.7)
If the detector is larger than the minimum size, and falls into
the N_A, N_H (below) class, N_{size} will scale like N_A, N_H
to the point where the minimum detector size is reached, and
like N_d, N_{amp}, below.

F. Housing Noise

When a detector is kept in a housing which radiates at
wavelengths to which the detector is sensitive, the detector
may be more strongly limited by this source of noise, N_H,
than by any other. When possible, the housing should
then be cooled, but in some applications that choice may
not be available, and this type of photon noise will then
dominate.

4.3.2   Optimum Operation

Let us now examine the best operating mode given the various sources of noise just mentioned. Amplifier noise does not guide us towards or away from spectral multiplexing. In general, a spectrum having m distinct elements requires m distinct measurements, whether we measure one spectral element at a time or all of them simultaneously. Either way therefore, a maximum time T may be available for any one measurement of the entire spectrum, and this will fix the noise level. It is clear, however, that in the presence of this type of noise, only one spectrum should be obtained in the available time interval. If two independent spectra of the source are taken in the available time, the signal-to-noise ratio of each one will be lowered by a factor of 2, and the sum of the spectra will be worse by $2^{1/2}$ than a single spectrum taken in the same time interval. This happens because the noise components of the summed spectra grow in random walk fashion while the signals add linearly. This argument, therefore, speaks against rapid scan spectra when the limiting noise is from the amplifier N_{amp}. In most other situations rapid scanning provides a succession of spectra which can help to average out effects of atmospheric and/or modulation noises. Since multiplexed spectrometers gather more light onto a detector in all cases, their use is still to be preferred when amplifier noise is present.

Let us next turn to the modulation noise component due to scintillation. Much of this noise can be avoided if a "total intensity" reference detector is used. In fact, this should always be done if modulation noise is suspected. The ratios of the instantaneous intensity measured by the reference detector should then be used as the primary spectral data. The only time that

such a procedure would not work is if the modulation is also wavelength dependent in an unpredictable way. Spectral multiplexing and high throughput are definite advantages if the ratio technique is employed. Otherwise, however, no advantage is gained by multiplexing. It is difficult to compensate for the atmospheric emission noise unless all signal time variations are attributed to this noise source and the reference detector signal is primarily used in a subtractive mode. Clearly, ambiguities arise when both atmospheric and modulation noise sources are present. If atmospheric noise is the dominant source of uncompensated noise, multiplexing will provide no advantage, and an unnecessarily high throughput will actually provide a disadvantage, since the noise may grow even faster than the signal.

If photon noise N_P dominates, Fellgett's advantage cannot be realized. By looking at m spectral elements simultaneously, the noise of each measurement increases as $m^{1/2}$. The total time T available for looking at each spectral element increases as m and since the noise components of successive measurements add randomly, the growth of noise will be proportional to $T^{1/2}$. The total noise, at the end of time T, therefore, is proportional to $m^{1/2}T^{1/2} = m$. The signal strength, integrated over this time interval, is also increased by a factor of m, and there is no net gain in signal-to-noise ratio through multiplexing.

Detector noise N_c always makes multiplexing worthwhile. Let the spectrum consist of m spectral elements and the noise for any one measurement lasting time T/m be n_1. Let the signal received in the same time interval be s. If each spectral element is seen for a total number of times $\frac{1}{2}m$, the signal at the end of the total observing period T will integrate to $\frac{1}{2}sm$. Since the noise is

4-8

present even when no signal falls onto the detector, the noise n_1 must be summed in random walk fashion over all m time intervals and integrates up to $n_1 m^{1/2}$. The SNR therfore improves by $\frac{1}{2} m^{1/2}$.

Since many detectors show increasing noise with increasing size, we must still examine how to optimally operate when area noise N_A dominates. In this case multiplexing must often be accompanied by "dedispersion", Fellgett (1958)[2]. Dedispersion consists in passing the radiation back through the spectrometer, once the modulation at the exit slit has taken place. Decker (1971)[9] has shown how this can be readily accomplished in practice. Dedispersion can gather all the radiation back onto an area as small as the entrance slit of the instrument and in principle no increase in detector size is then implied by multiplexing. Just as for detector noise, Fellgett's advantage holds in this situation. If the radiation is not dedispersed, a bigger detector is needed. The noise increases as $A^{1/2}$, the effective time increase for viewing the signal goes up by $\frac{1}{2} A$ and the SNR decreased by $\frac{1}{2}$ - it actually is lowered!

4.3.3   Computation and Construction Tolerances

Two final characteristics which must be included in any compari-son of spectrometric instruments are the computational complexity required to produce a usable spectrum and the construction tolerances necessary to insure correct operation. Both of these requirements are at a minimum for conventional scanning-mono-chrometer spectrometers: there is no necessarv post-measure-ment computation whatever, and, with the exception of the initial manufacture of the diffraction grating, the constructional tolerances are merely those normally associated with the construction of conventional optical systems.

In the area of computational complexity, the Hadamard-transform spectrometer has a clear advantage over other multiplex systems. In principle, the Fast Hadamard Transform runs approximately an order of magnitude faster than the equivalent Fast Fourier Transform, per transform dimension, Pratt et. al., (1969). When one takes into account the fact that Hadamard spectrometers typically operate with much smaller multiplex numbers than do Fourier spectrometers, and hence require the decoding of a much smaller data matrix, Hadamard-transform spectrometers typically require far less in terms of computer power and computer time than do Fourier-transform spectrometers. For instance, a typical FTS system might involve a minicomputer with 16k to 32k of core memory and also a high-speed disc memory containing up to 1 million additional words; a typical Hadamard system might involve either a stripped-down minicomputer or a microprocessor,

either with only 4k to 7k of core memory (and no disc or tape memory at all). In addition, the Hadamard transform lends itself to inversion by simple, special-purpose, real-time "hard-wired" computers or systems based on microprocessor chips and read-only memories, Slingerland, (1975).

Similarly, in the area of mechanical complexity and construction tolerances, the Hadamard spectrometer shows a clear advantage over other multiplex spectrometric systems. Fourier spectrometers, as they are interferometric instruments, require not only fraction-of-wavelength-of-light accuracy in the motion of the variable-length arm of the interferometer, but for satisfactory operation, also require the use of up to 3 separate interferometers operating simultaneously: the signal (infrared) interferometer, a reference interferometer looking at a helium-neon laser (to calibrate the interferometer fringes and synchronize the data

system), and a "white-light" interferometer (to provide proper phasing of the "zero order fringe"). Hadamard spectrometers, by contrast, require only conventional optical tolerances, except for the diffraction grating and the multislit code mask - which, of course, need only be manufactured once. Typically, then, HTS systems require construction and operation tolerances of the order of fractions of millimeters, while FTS systems require tolerances of the order of fractions of micrometers.

4.3.4   Echo-Correction

Closely related to the matter of construction tolerances is the matter of error susceptibility and error correction capability.

All multiplex systems are in one respect improvements over conventional scanning spectrometers, in that partial data loss produces only degredation of the overall signal-to-noise ratio of the spectrum, while similar partial data loss with scanning spectrometers result in "gaps" in the spectrum - total loss of information about the particular spectral region under study during the time of the data loss. The other side of that coin, as it were, is that all multiplex systems distribute isolated high-noise "bursts" throughout the entire spectrum, degrading its signal-to-noise, while monochrometers inherently isolate noise bursts to the specific spectral regions during which they occurred, rendering those areas essentially illegible, but preserving the signal-to-noise of the remainder of the spectrum.

One can further ask what types of operational or manufacturing errors are most probable for a given type of system, what their effects would be on the resulting spectra, and what (if anything) can be done about the situation.   The most probable error to

which the Hadamard spectrometer is subject would be one in the construction or motion of the encoding mask. Small random errors will, to first order, merely degrade the final spectral signal-to-noise ratio, and are not susceptable to systematic correction.

Systematic errors in the construction (or motion) of the multislit coding mask will, however, result in a systematic pattern of "echos" in the output spectrum, (Tai, et. al., (1975b). Tai and his co-workers showed that for masks whose transparent slits are systematically wider or narrower than they should be, a single input spectral line will be distorted to an output spectrum containing that "correct" line plus a set of small "echos". When the transparent slits are too wide, these echos are of equal height, and generally consist of one pair surrounding the line and a second pair bunched together and displaced a definite specific distance from it; when the slits are too narrow, both sets of echos still have the same amplitude, but the displaced echos are negative. The location of the echos is uniquely determined by the code design of the mask, and hence is the same for all masks of a given design. The amplitude and sign of the echos; their position is determined by the mask code itself! For instance, in the common case of an HTS mask of 255 slits, an error in the slit width shows up as a pair of echos spaced 24 and 25 spectral channels from the input line; if the slits are too wide, all four echos are "positive" (same as correct line), if too narrow, the echos displaced 24 and 25 channels are negative.

As the effect of error in the coding mask can be uniquely related to the single-spectral-line response of the spectrometer, it is thus possible to correct for the effects of this error in the process of the computer decoding; Tai et. al, (1975b) have devised such

a correction procedure. This procedure consists of essentially three steps: First, a single-line spectrum is run with the code mask under consideration, to determine the amplitude and sign of any errors present, and the appropriate scaling constant of the echos is calculated; this need only be done once during the initial system calibration for any instrument. Next, the decoding program is modified so that it constructs a second "replica" of each (arbitrary) transformed spectrum, where the "replica" has been multiplied by the echo scaling factor determined during initial calibration. This scaled replica is then "cycled" through the spectrum and added (or subtracted, depending on the sign of the mask error) from the original spectrum so that each spectral point has had added (or subtracted) from it the scaled values corresponding to the known echo locations. This sounds complicated, but can, in fact, be accomplished with 4 or 5 additional lines in the FORTRAN "decoding" program.

Figure 4-1 shows the effect of this correction on the spectrum of an 11.018μ line-filter taken with a 255-slot Hadamard-transform spectrometer. The mask error was approximately 5% of the width of an individual slit, or about 0.008 mm, and the resulting echos have been corrected to far less than the spectral noise level.

This capability to correct for the dominant system error as part of the routine decoding procedure is unique to Hadamard spectrometry; Fourier spectrometry errors are seldom correctable and typically result in degredation of spectral quality.

4.3.5 Spectral Manipulation

We would like to add a final note on one "multiplex advantage" which Hadamard shares with all other multiplex spectral techniques: the ease of post-measurement spectral manipulation,

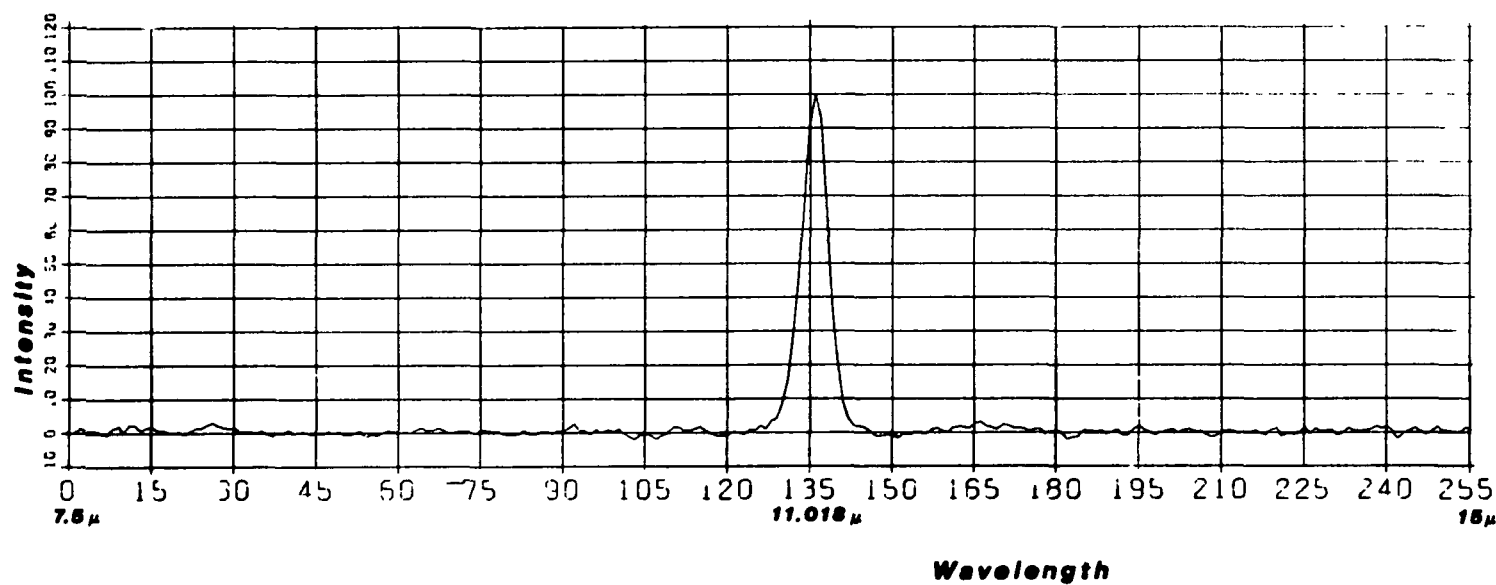# Uncorrected Spectrum

T21
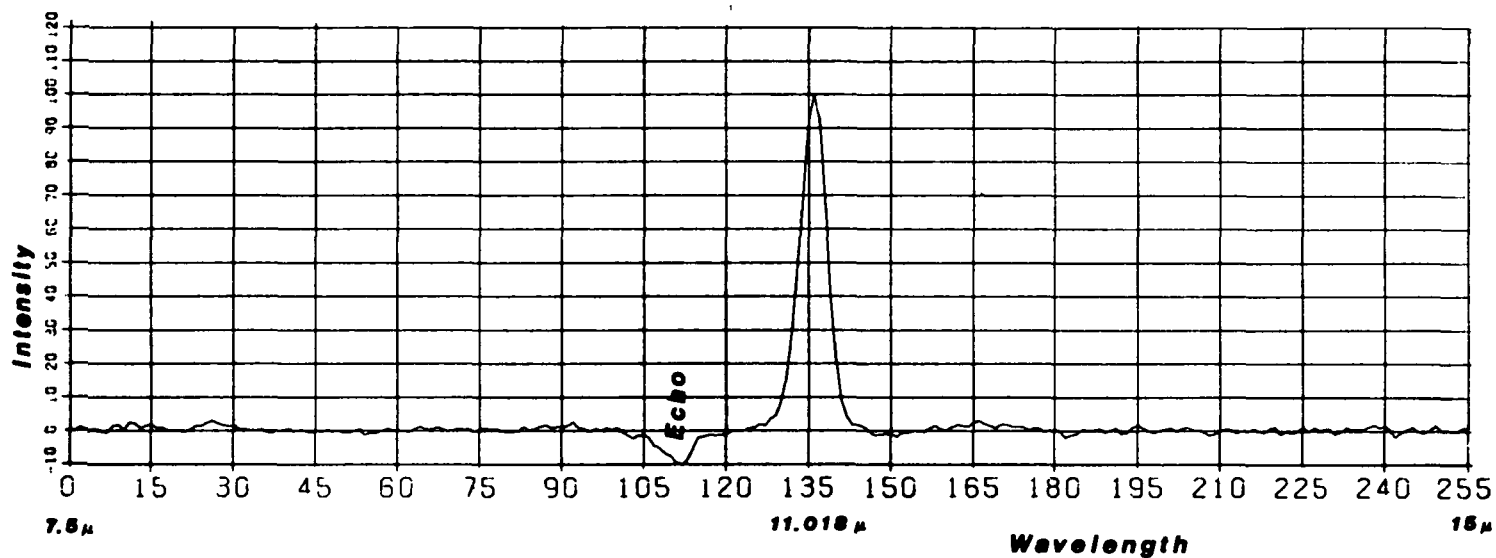
Echo-Corrected Spectrum

T21

Fig. 4-1. Mask-Error-Echo correction of HTS spectra (11.018μ line-filter source).

due to the necessary use of a digital computer in the measurement cycle. In both Fourier and Hadamard spectrometry, the output spectrum exists in the computer memory as an array of numbers, and hence is available for ensemble spectral averaging, normalization, ratioing, feature subtraction, mixture reduction or any other mathematical manipulation desired by the experimenter. This has been described, among others, by Griffiths (1974) and Hirschfeld (1976) and is one of the major reasons for the growing acceptance of Fourier techniques among analytical spectrochemists.

We wish to note here that these manipulative possibilities are fully applicable to Hadamard spectrometry. As one example, we refer to Figure 4-2: the upper trace (D4) is a single-beam spectrum of polystyrene film, seen in the region from 7.5 to 15μ, which is seen superimposed upon a source spectrum (R9, central trace) containing, among other things, a sharp order-sorting-filter "cut-on" and a rather deep "resonance" from this filter. The lower trace (D4/R9) shows the effect of computer ratioing of the sample spectra with the stored IR source "reference" spectrum to produce a "corrected" sample spectrum.

4.4   Hadamard Mask Design

4.4.1   Mask Description

A standard Hadamard mask utilizes a cyclic code which makes it possible to construct a single double-length multislit mask which contains all of the patterns necessary to encode the spectrum. Since, in the HROM instrument, the spectral bands of interest are not contiguous and are not equally spaced, a standard cyclic Hadamard mask cannot be used. Instead, a discrete field stop which contains the monochrometer exit slits that define the required twelve spectral bands, must be
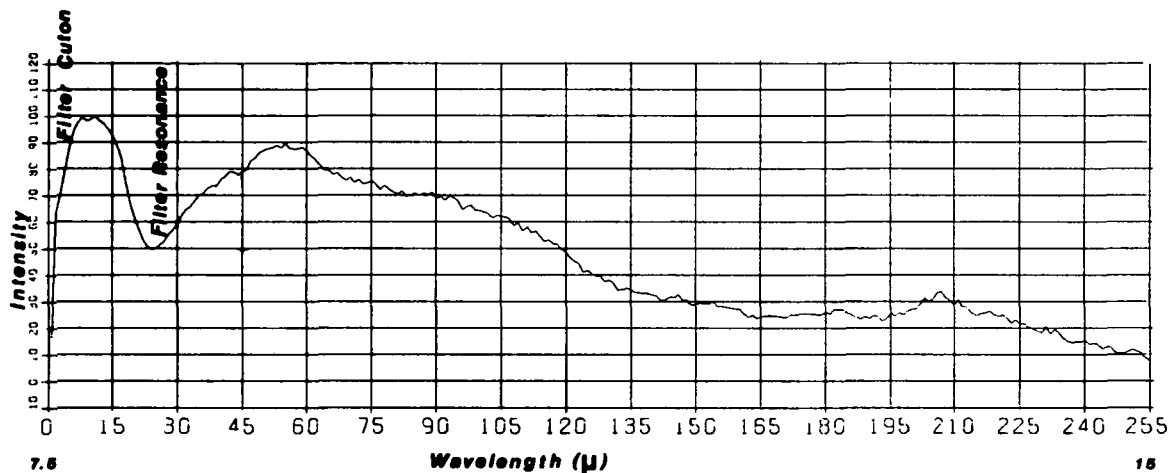
Polystyrene Film D4

Wavelength (μ)

IR Source R9

Wavelength (μ)
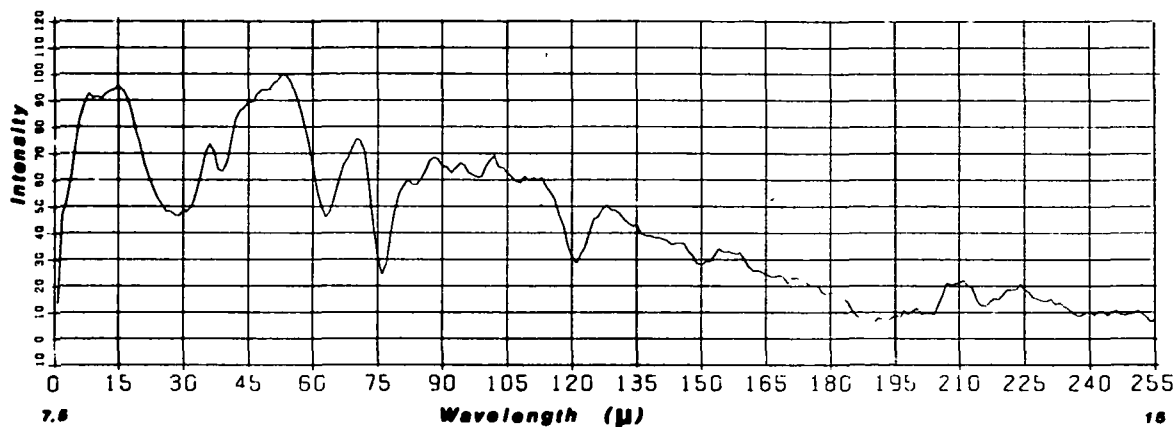
Polystyrene Film
divided by
IR Source D4/R9
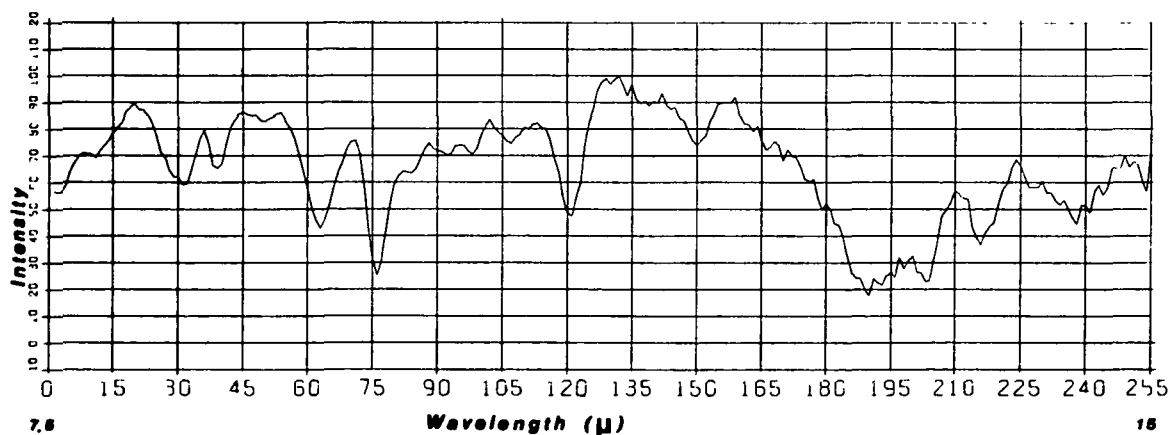

Wavelength (μ)

Fig. 4-2   Compensation of sample spectra (here, Polystyrene film) by computer ratioing to stored reference spectra (here, IR glower source).

used in conjunction with a Hadamard mask. The field stop is shown in Figure 4-3. Following the field stop is the Hadamard mask. This mask moves normal to the dispersion direction and uses a separate pattern for each measurement. Thus, the total mask is composed of n individual patterns. The slits on the mask line up with the exit slits in the field stop as shown in Figure 4-3. Use of the field stop reduces the accuracy requirements on the Hadamard mask, since the spectral bands are defined by the field stop.

4.4.2 Selected Code

The code selected for this application is a 15 slot cyclic code, having the form:

10001 0011010111

The complete code for all 15 positions is shown in Figure 4-4. Since the code has 15 positions, and the instrument only requires 12, an inefficiency is present. To remove this inefficiency, three imaginary spectral bands are measured λ_{13}, λ_{14}, and λ_{15}. These three bands equal 0. However, by using these bands, 15 measurements of 15 unknowns are performed, and the inefficiency is removed

4.4.3 Mask Size

The radius of the Hadamard mask is determined from the following formula:

$$R_d = \frac{1.2\ H_s}{2 \tan \dfrac{360^o}{2n}} + \frac{\Delta\lambda\ A_s}{\Delta\gamma\ H_s} \qquad (4.8)$$

FIELD STOP

0.74mm

20.68mm

62.37mm

0mm   12.96   23.11   30.24   54.51 62.37
         19.80   26.42   33.41

HADAMARD MASK

SLOT
POSITIONS   ~ 0.89mm

POSITION
1

POSITION
2

~ 24mm

MASK
MOVES
UP

POSITION
n

Fig. 4-3   Hadamard Mask and Field Stop

```
10001 00110 10111
00010 01101 01111
00100 11010 11110
01001 10101 11100
10011 01011 11000

00110 10111 10001
01101 01111 00010
11010 11110 00100
10101 11100 01001
01011 11000 10011

10111 10001 00110
01111 00010 01101
11110 00100 11010
11100 01001 10101
11000 10011 01011
```

Fig. 4.4   Hadamard Code

where:

H_s = The height of the slits

1.2 = Factor which makes slits 20% oversized

n = Number of mask positions = 16

$\dfrac{\Delta\lambda W_s}{\Delta\gamma}$ = Focal plane width

$\Delta\lambda$ = Total spectral range = 3398 Å - 2555 Å = 843Å

$\Delta\gamma$ = Spectral resolution = 10Å

W_s = Width of slits = $\dfrac{A_s}{H_s}$

A_s = Area of slit = 0.153 cm^2

The proposed mask contains 15 positions for the Hadamard code and one blank position. The blank position is used to measure a dark noise every frame. Thus, the number of mask positions is 16. In section 4.5 the area of the slits A_s required for a 30/1 signal-to-noise ratio is defined as 0.153 cm^2. Therefore, substituting values into the equation, we get:

$$R_d = 3.0164\ H_s + \frac{12.8979}{H_s} \qquad (4.9)$$

This equation is tabulated in Table 4-1. Where H_s is the slit heights, W_s is the slit widths, L is the width of the focal plane and R_d is the radius of the Hadamard mask wheel. The equation is also plotted on Figure 4-5. Notice that there is an optimum value for a given area slit. For the proposed mask, the slit height is 2.068 cm, the slit width is 0.074 cm and the radius of the wheel is 12.475 cm.

4 - 20

TABLE 4.1

Hadamard Mask Parameters

Hs cm	(in.)	Ws cm	(in.)	L cm	(in.)	Rd cm	(in.)
1.0	(0.394)	0.153	(0.060)	12.898	(5.078)	15.914	(6.265)
1.25	(0.492)	0.122	(0.048)	10.318	(4.062)	14.089	(5.547)
1.50	(0.591)	0.102	(0.040)	8.599	(3.385)	13.124	(5.167)
1.75	(0.689)	0.087	(0.034)	7.370	(2.902)	12.649	(4.980)
2.0	(0.787)	0.076	(0.030)	6.449	(2.539)	12.482	(4.914)
2.068	(0.814)	0.074	(0.029)	6.237	(2.455)	12.475	(4.911)
2.10	(0.827)	0.073	(0.029)	6.142	(2.418)	12.476	(4.912)
2.25	(0.886)	0.068	(0.027)	5.732	(2.257)	12.519	(4.929)
2.50	(0.984)	0.061	(0.024)	5.159	(2.031)	12.700	(5.000)
2.75	(1.083)	0.056	(0.022)	4.690	(1.846)	12.985	(5.112)
3.0	(1.181)	0.051	(0.020)	4.299	(1.693)	13.348	(5.255)
3.25	(1.279)	0.047	(0.019)	3.969	(1.562)	13.772	(5.422)
3.50	(1.378)	0.044	(0.017)	3.685	(1.451)	14.242	(5.607)
3.75	(1.476)	0.041	(0.016)	3.439	(1.354)	14.751	(5.807)
4.0	(1.575)	0.038	(0.015)	3.224	(1.269)	15.290	(6.020)

$$Rd = 3.0164Hs + \frac{12.8979}{Hs}$$

Fig. 4-5
Hadamard Mask Parameters

RADIUS OF DISC (R_d)

DISTANCE FROM CENTER

FOCAL PLANE SIZE (L)

SCALE IN CENTIMETERS

HEIGHT OF SLITS (H_s cm)

4 - 22
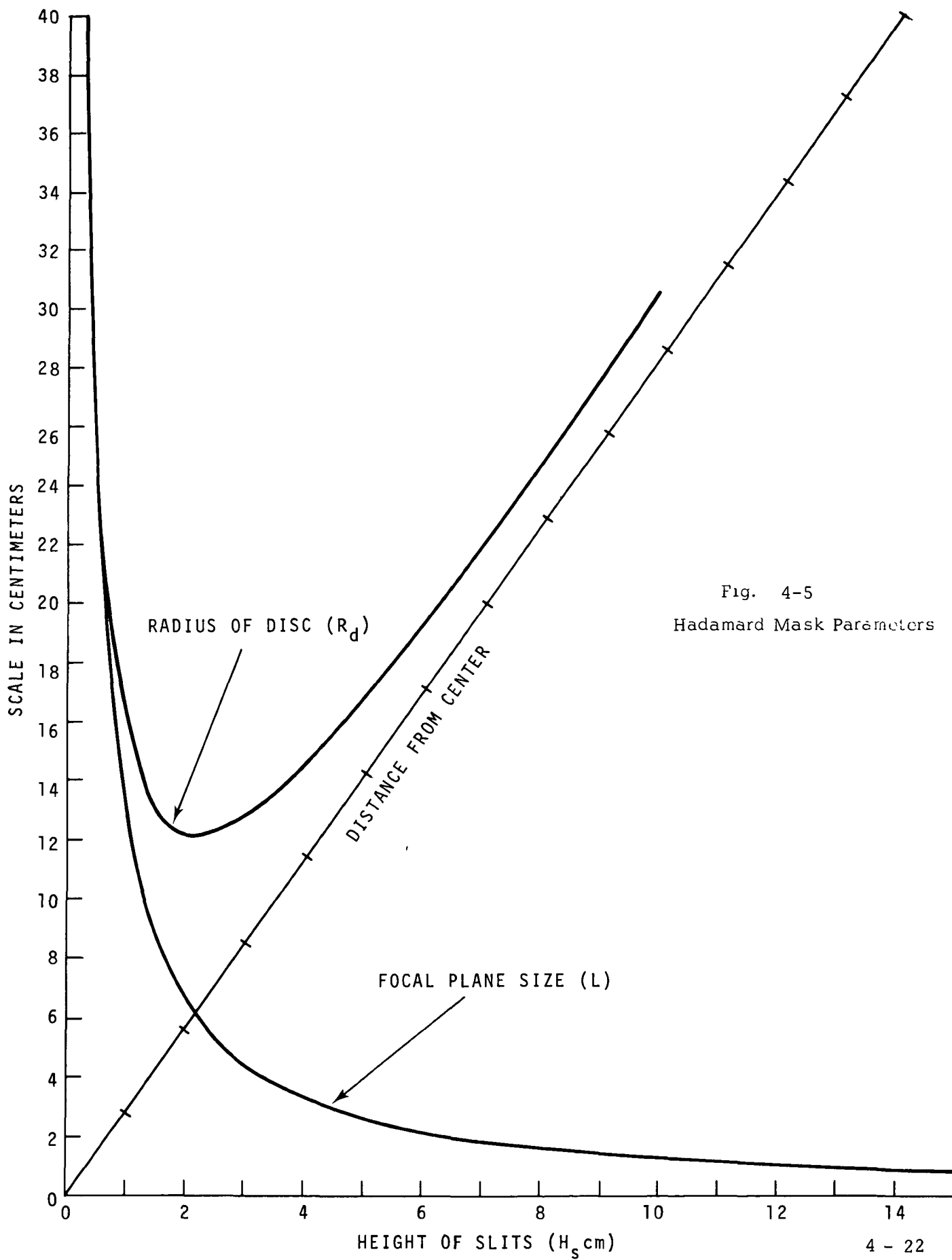
4.5   Performance Comparison

Since the conventional spectral scanner is based on the BUV instrument and the Hadamard spectral scanner has just been shown to be possible, it remains to compare the two sensors from a performance viewpoint. The two systems will be compared again using signal-to-noise ratio. However, this time the values used in the equations will be based on realistically derived system parameters.

4.5.1   Number of Photoelectrons in the Signal (N_S)

The number of photoelectrons in the signal can be calculated from the formula:

$$N_S = \frac{NA_S \ \Omega \ \tau_O \ \Delta \nu \ \lambda \ \eta_q \ 10^{-7}}{hc} \qquad (4.10)$$

where N =   Scene radiance - given in work statement as 2.5×10^{-4} erg/cm^2 - sr - $\overset{o}{A}$ - s

A_S =   Area of slits = 2.137 cm high by 0.072 cm wide

Ω =   Solid angular field of view = $7^o \times 7^o$ = 0.01493 sr (given in work statement)

$\Delta\nu$ =   Spectral resolution = $10\overset{o}{A}$ (given in work statement)

τ_O =   Optical efficiency = 2% (same as present BUV)

λ =   Wavelength of interest = $2555\overset{o}{A}$ = 0.2555μm

η_q =   Quantum efficiency of PMT @ $2555\overset{o}{A}$ = 15% (PMT catalogue valve)

10^{-7} =   Conversion factor ergs to watt. sec.

h =   Planck's Constant = 6.625×10^{-34} w - sec^2

c =   Speed of light = 2.99793×10^{14} μm/sec

Substituting the values into equation (4.10) we get:

$$N_s = \frac{(2.5 \times 10^{-4})(0.154)(0.0149)(0.02)(10)(0.2555)(0.15)(10^{-7})}{(6.625 \times 10^{-34})(2.99793 \times 10^{14})}$$

$$N_s = 2.21 \times 10^3 \text{ photoelectrons/sec.}$$

4.5.2 Bandwidth (Δf_n)

The noise bandwidth for the two systems can be calculated from the following expression:

$$\Delta f_n = \frac{\Theta_x \, \Theta_y \, \Theta_\lambda \, F_T}{2 n_d \, K \, \omega_x \, \omega_y \, \omega_x} \qquad (4.11)$$

where

Θ_x	=	Total field of view in the x direction = $104°$
Θ_y	=	Total field of view in the y direction = $7°$
Θ_λ	=	Total spectral range 2555 to $3398\overset{o}{A}$ = $843\overset{o}{A}$
ω_x	=	Instantaneous field of view in the x direction = $7°$
ω_y	=	Instantaneous field of view in the y direction = $7°$
ω_λ	=	Spectral resolution = $10\overset{o}{A}$ for each of 12 bands
$\dfrac{\Theta_x}{\omega_x}$	=	15 resolution elements (pixels) per line
$\dfrac{\Theta_y}{\omega_y}$	=	1 resolution elemt high
$\dfrac{\Theta_\lambda}{\omega_\lambda}$	=	16 spectral bands (bands λ_{13}, λ_{14}, and $\lambda_{15} = 0$) for the Hadamard system and 12 spectral bands for the conventional system
F_T	=	Number of frames per second = $1/7.38$ sec.
n_d	=	Number of photomultiplier channels = 15
K	=	Scan efficiency - 98% (0.01 sec per $22.5°$ step for Hadamard mask) 75% (littrow type mirror for conventional system).

4 - 24

substituting the values into equation 5.2 we get:

$$\Delta fn_H = \frac{(15)\ (1)\ (16)}{2\ (15)\ (.98)\ (7.38)}$$

$$\Delta fn_H = 1.106\ Hz \quad \text{For the Hadamard System}$$

$$\Delta fn_C = \frac{(15)\ (1)\ (12)}{2\ (15)\ (.75)\ (7.38)}$$

$$\Delta fn_C = 1.084\ Hz \quad \text{For the Conventional System}$$

4.5.3   Signal-To-Noise Ratio (S/N)

A.   Hadamard System (s/n)H

The signal-to-noise-ratio for a Hadamard System was derived in section 3.3.2 and is:

$$\left(\frac{S}{N}\right)_H = \frac{N_s\ (MP)^{1/2}}{2N\ \Delta fn_H^{1/2}\left[\dfrac{N_s\ MP}{2N}+N_D\right]^{1/2}} \tag{4.12}$$

where

$(S/N)_H$ =   Signal-to-noise ratio for a Hadamard System = 30 (given in work statement)

N_s =   Number of photoelectrons in the signal = 2.21×10^3 pe/sec (calculated in Section 5.1.1)

P   =   Number of spectral bands = 16 (12 from work statement, λ_{13}, λ_{14} and $\lambda_{15}=o$)

M   =   Number of spatial resolution elements = 1 (15 PMT's, one pixel per tube)

N   =   Number of Hadamard masks = 1

Δfn_H =   Noise bandwidth for a Hadamard System = 1.106 Hz (calculated in Section 5.1.2)

N_D =   Number of photoelectrons from additive noise = ?

Solving equation (4.12) for N_D and substituting values of 1 for M and N. The equation becomes:

$$N_D = \frac{N_s P}{2} \left[\frac{N_s}{2\left(\frac{S}{N}\right)^2_H \Delta fn_H} - 1 \right]$$

(4.13)

Substituting values into equation (4.13) we get:

$$N_D = \frac{2210(16)}{2} \left[\frac{2210}{2(30)^2 (1.106)} - 1 \right]$$

$$N_D = 1.947 \times 10^3 \text{ photoelectrons/second.}$$

1) $N_s >> N_D$

For noise in signal limited operation equation (4.12) reduces to:

$$\left(\frac{S}{N}\right)_H = \frac{N_s^{1/2}}{\left[2 \Delta fn_H\right]^{1/2}}$$

(4.14)

and substituting values into equation (4.14) we get:

$$\left(\frac{S}{N}\right)_H = 31.61 \text{ when } N_s >> N_D$$

2) $N_s < N_D$

For additive noise limited operation equation (4.12) does not change. Substituting values into the equation and letting $N_D = 1.62 \times 10^4$ pe/sec the signal-to-noise ratio becomes:

$$\left(\frac{S}{N}\right)_H = 22.83 \quad N_D > N_s$$

3) $N_S = N_D$

When the additive noise in signal are equal equation (4.12) does not change. Substituting values into equation (4.12) and letting $N_D = N_s$ the signal-to-noise ratio becomes:

$$\left(\frac{S}{N}\right)_H = 29.80 \quad N_s = N_D$$

B.   Conventional System $(S/n)c$

The signal-to-noise ratio equation for a convention system is:

$$\left(\frac{S}{N}\right)_c = \frac{N_s}{\Delta fn_c^{1/2}\left[N_s + N_D\right]^{1/2}} \tag{4.15}$$

where the symbols are the same as for the Hadamard System and the values are the same except for Δfn_c which equals 1.084 Hz.

Solving equation (4.15) for N_D we get:

$$N_D = N_s\left[\frac{N_s}{\left(\frac{S}{N}\right)_c^2 \Delta fn_c} - 1\right] \tag{4.16}$$

substituting values into equation (4.16) we get:

$$N_D = 2.796 \times 10^3 \text{ pe/sec}$$

1) $N_S >> N_D$

For noise in signal limited operation equation (4.15) reduces to:

$$\left(\frac{S}{N}\right)_c = \frac{N_s^{1/2}}{\Delta fn_c^{1/2}} \tag{4.17}$$

Susstituting values into equation (4.17) we get:

$$\left(\frac{S}{N}\right)_c = 45.15 \text{ when } N_S >> N_D$$

2) $N_S < N_D$

For the additive noise limited case-equation (4.15) does not change.

Substituting values into the equation and letting $N_D = 1.62 \times 10^4$ pe/sec the signal-to-noise ratio reduces to:

$$\left(\frac{S}{N}\right)_c = 15.64 \quad \text{For } N_D > N_S$$

3) $N_S = N_D$

When the additive noise and the noise in signal are equal, equation (4.15) does not change. Substituting values into equation (4.15) and setting $N_S = N_D$ the signal-to-noise ratio becomes:

$$\left(\frac{S}{N}\right)_c = 31.93 \quad \text{For } N_S = N_D$$

C. Crossover Point

At what value is the signal-to-noise ratio for the Hadamard System equal to that of the convention systems? This value can be found by equating equations: (4.12) and (4.15) as follows:

$$\left(\frac{S}{N}\right)_H = F \left(\frac{S}{n}\right)_c \qquad (4.18)$$

since

$$\left(\frac{S}{N}\right)_H = \frac{N_S P^{1/2}}{2 \Delta fn_H^{1/2} \left[\frac{N_S P}{2} + N_D\right]^{1/2}} \qquad (4.19)$$

and

$$\left(\frac{S}{N}\right)_c = \frac{N_S}{\Delta fn_c^{1/2} \left[N_S + N_D\right]^{1/2}} \qquad (4.20)$$

$$\therefore \quad \frac{N_S P^{1/2}}{2 \Delta fn_H^{1/2} \left[N_S P/2 + N_D\right]^{1/2}} = \frac{F N_S}{\Delta fn_c^{1/2} \left[N_S + N_D\right]^{1/2}} \qquad (4.21)$$

rearranging equation (4.21) we get:

$$P^{1/2} = \frac{2\,F\,\Delta fn_H^{\ 1/2}\left[N_s P/_2 + N_D\right]^{1/2}}{\Delta fn_c^{\ 1/2}\left[N_s + N_D\right]^{1/2}} \tag{4.22}$$

and

$$P^{1/2}\left[N_s + N_D\right]^{1/2}\Delta fn_c^{\ 1/2} = 2\,F\Delta fn_H^{\ 1/2}\left[\frac{N_s P}{2} + N_D\right]^{1/2} \tag{4.23}$$

squaring both sides of equation (4.23) gives:

$$P\left[N_s + N_D\right]\Delta fn_c = 4F^2\,\Delta fn_H\left[N_s P/_2 + N_D\right] \tag{4.24}$$

Performing the multiplication indicated in equation (4.24) yield:

$$P\Delta fn_c\,N_s + P\,\Delta fn_c\,N_D = 4F^2\Delta fn_H\,\frac{N_s P}{2} + 4F^2\,\Delta fn_H \tag{4.25}$$

Collecting like terms in equation (4.25) we get:

$$2F^2\Delta fn_H\,N_s P - P\Delta fn_c\,N_s = P\Delta fn_c\,N_D - 4F^2\Delta fn_H \tag{4.26}$$

Factoring equation (4.26) gives:

$$N_s P\left[2F^2\Delta fn_H - \Delta fn_c\right] = N_D\left[P\Delta fn_c - 4F^2\Delta fn_H\right] \tag{4.27}$$

Solving equation (4.27) for N_D we get:

$$N_D = \frac{N_s P\left[2F^2\Delta fn_H - \Delta fn_c\right]}{\left[P\Delta fn_c - 4F^2\Delta fn_H\right]} \tag{4.28}$$

If we let

$P = 15, \Delta fn_H = 1.106\ H_z,\ \Delta fn_c = 1.084$ and $N_s = 2210$ pe/sec

and substitute these values into equation (4.28) we get:

$$\frac{35360\left[2.212F^2 - 1.084\right]}{\left[17.344 - 4.424\ F^2\right]} \tag{4.29}$$

Finally since $\left(\dfrac{S}{N}\right)_H = \left(\dfrac{S}{N}\right)_C$; $F = 1$,

$$N_D = 3.09 \times 10^3 \text{ pe/sec} \qquad \left(\dfrac{S}{N}\right)_H = \left(\dfrac{S}{N}\right)_C$$

4.5.4 <u>Conclusion</u>

Figure 4-6 shows the signal-to-noise ratio for a Hadamard System and a conventional system as a function of additive noise. Notice that the conventional system starts out with a better S/N ratio however when the additive noise level reaches 3090 pe/sec. , the two are equal and if more noise is added the Hadamard System excels. Again, as in Section 3, the signal-to-noise ratio cannot be used directly to select a final candidate system.
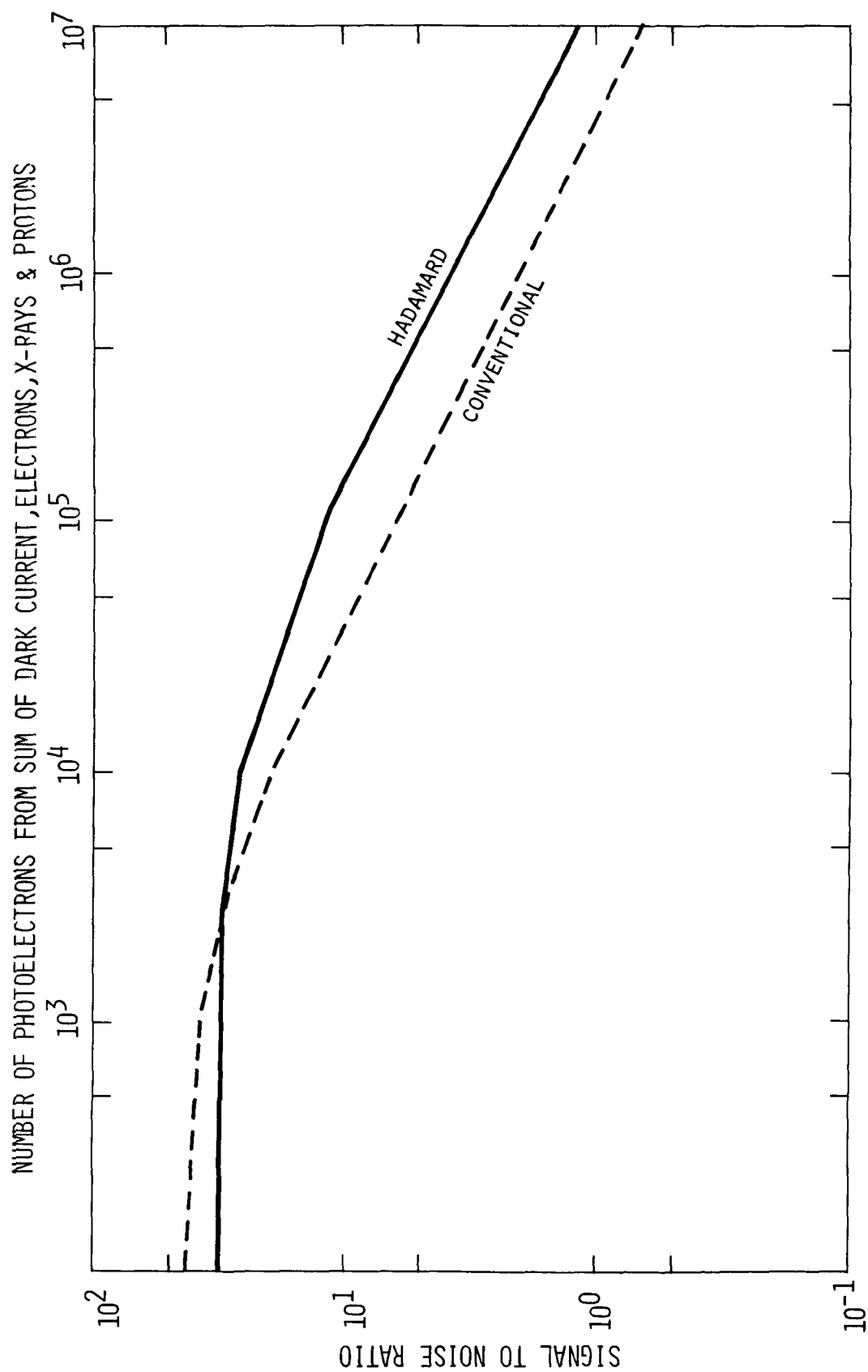
Figure 4-6   Signal-to-Noise Ratio vs Number of Photoelectrons from Additive Noise for a Constant Value of Signal Photoelectrons (N_s).

5. 0   SELECTION OF RECOMMENDED SYSTEM

5. 1   System Comparison

Having completed the performance evaluation (Section 4. 0) and
shown that either system can be characterized, it now remains to
determine which system is preferred, both from considerations of
performance and engineering simplicity.

5. 1. 1   Performance

Since the only difference in the two systems is the spectral
scanning, most of the performance criteria can be met equally
by both systems. These include such items as precision,
dynamic range, calibration, linearity, fidelity and thermal
influence. From a signal-to-noise ratio standpoint, either
system can meet the 30 to 1 requirement. However, the
conventional system is superior when noise-in-signal limited
and the Hadamard is superior when additive noise limited.
However, calculations show that the additive noise will be
above the crossover point. Therefore, the Hadamard system
is slightly superior.

5. 1. 2   Engineering Simplicity

Both systems use light pipes and 15 photomultipliers, 15 ampli-
fiers, 15 A to D converters and 15 processing electronics; thus,
electronically they are similar. From a telemetry standpoint,
the Hadamard code has an advantage, since dropped bits or
words only manifest themselves as a general lowering of the
signal-to-noise ratio of the decoded scene, not as loss of
information. Also, the simple rotary motion of the encoding
disc is easier to mechanize than the oscillating motion required
for conventional spectral scanning.

5. 1. 3 Recommended System

The recommended system is the pushbroom scanner for spatial scanning and the Hadamard Scanner for spatial scanning. The selection was made on the basis of a slight performance advantage and a more substantial advantage in mechanization.

6. 0   SYSTEM MECHANIZATION

6. 1   System Description

The design of the HROM sensor is based on the experience
gained from the BUV instrument flown on NIMBUS 4. An
outline drawing of the HROM instrument is shown on figure 6. 1.
Basically, the HROM system is composed of the entrance
optics which define the instrument field of view and direct the
incoming radiation onto the first collimating mirror. The
collimated energy is directed to the first grating where the
radiation is dispersed. The dispersed energy is then recollimated
and dispersed again by a second grating. The doubly dispersed
radiation is then encoded by the Hadamard spectral mask,
collected by light pipes and transmitted to the photomultipliers.
The light pipes collect the spectrally encoded radiation in such
a manner that the spatial orientation is preserved. Outputs
from the photomultipliers go to separate signal processing
electronics and on to logarithmic A/D converters that interface
with the spacecraft telemetry.

6. 2   Optical Design

The basic design of the optical system is very similar to that
of the BUV instrument flown on NIMBUS 4 and the SBUV scheduled
for NIMBUS G and is shown in Figure 6. 2.

The BUV spectrometer is an F/5 double Ebert-Fastie mono-
chromator using two 2400 1/mm gratings and two 250 mm focal
length spherical collimating mirrors. Double dispersion is
achieved at the exit slits by using three-corner-mirror transfer
optics between the two monochromators, which makes the
dispersion of the second monochromator additive. The use of

EXIT SLIT

AFT OPTICS HOUSING

LIGHT PIPES

PHOTO MULTIPLIERS

MONOCHROMATOR HOUSING

DIFFUSER MOTOR

ENTRANCE OPTICS AND DIFFUSER ASSEMBLY

ENTRANCE SLIT

CHOPPER

GRATING

COLLIMATING MIRRORS
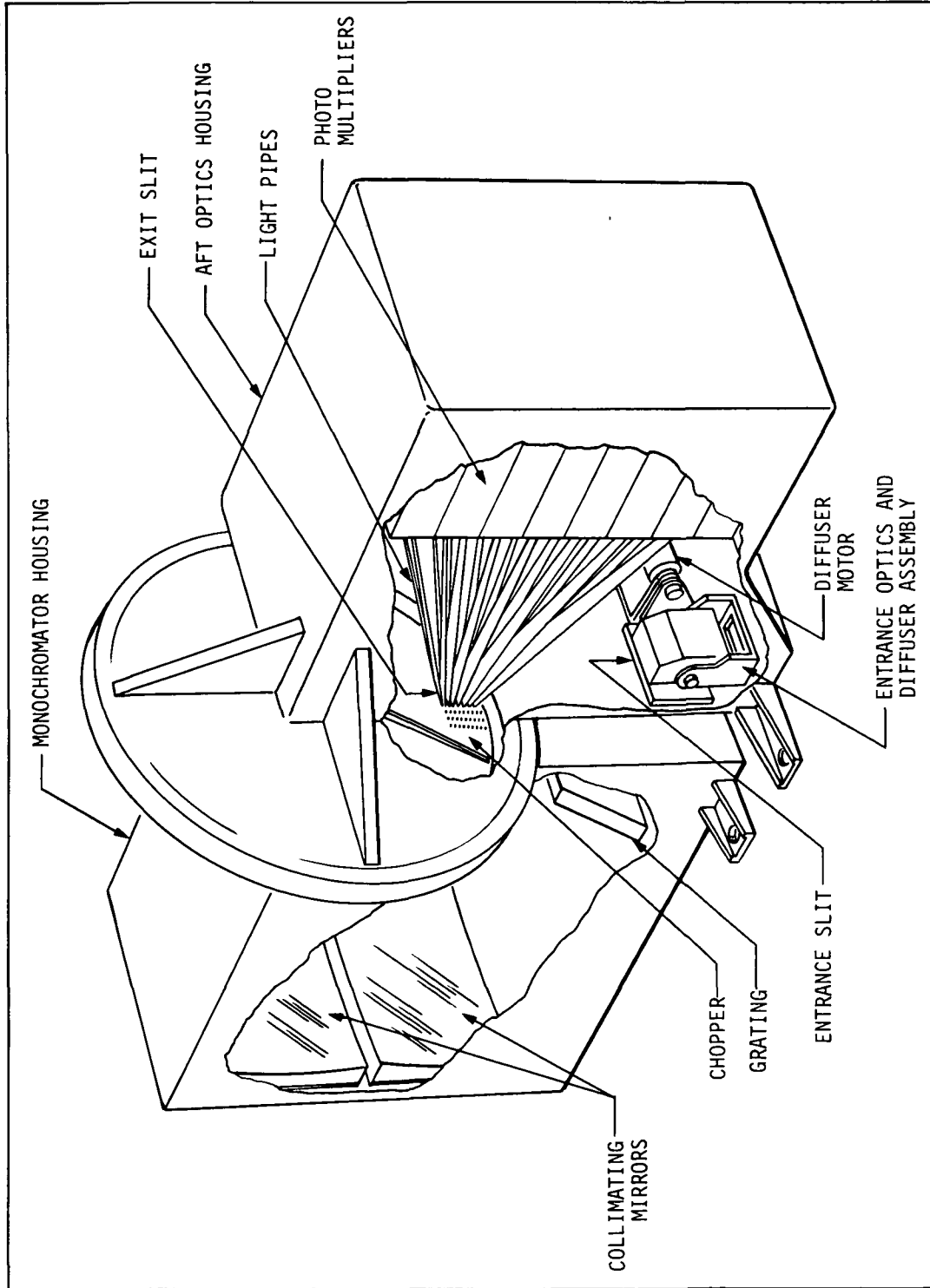
Figure 6.1   HROM Instrument

ELECTROMETERS + HIGH
VOLTAGE POWER SUPPLY

COLLIMATING
MIRRORS

CHOPPER DRIVE MOTOR

HADAMARD CHOPPER

LIGHT PIPES

GRATINGS

ENTRANCE LENS

TRANSMITTING DIFFUSER

PHOTOMULTIPLIERS
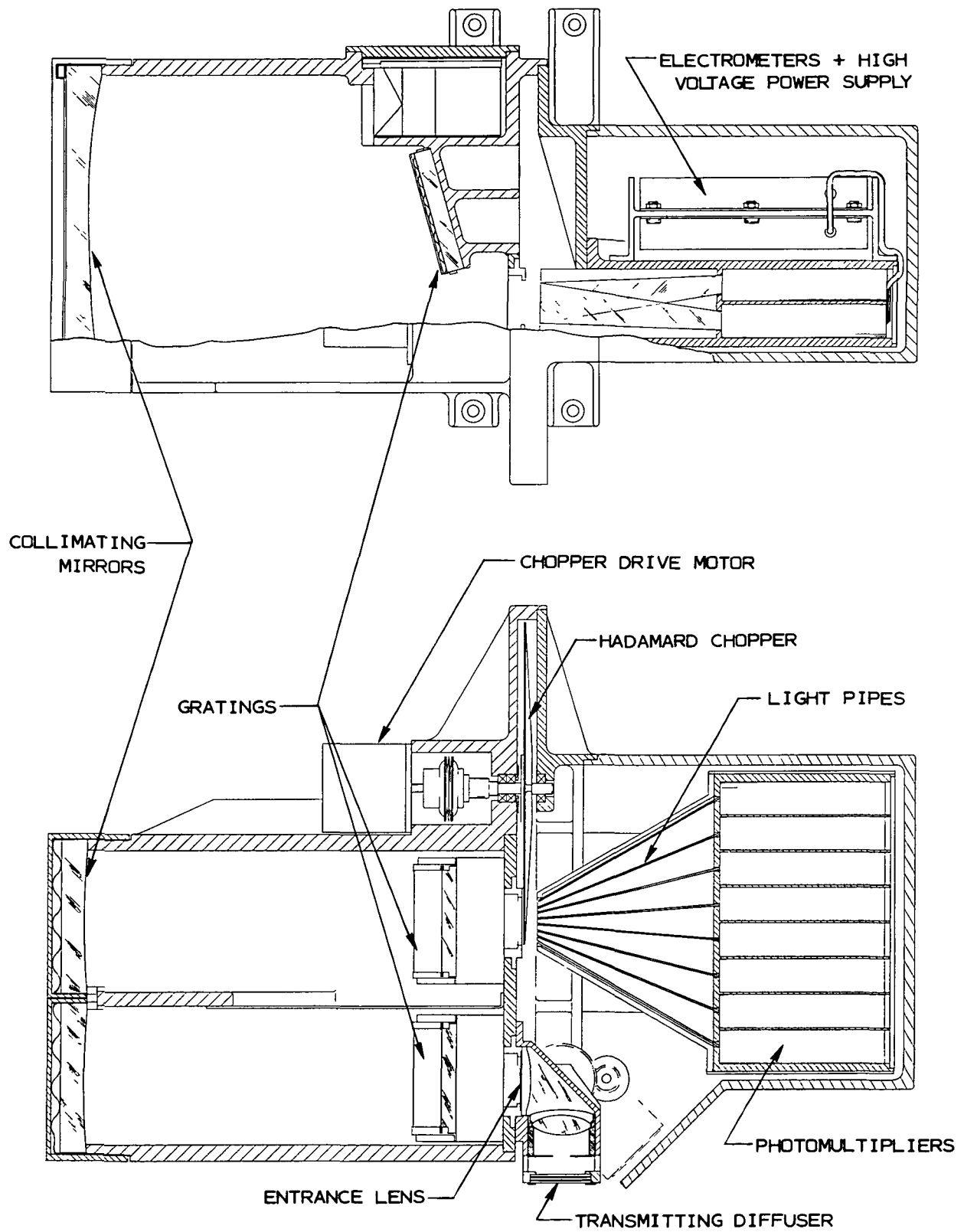
Figure 6. 2   Layout Drawing ot HROM

double dispersion with a double monochromator system permits
the entrance and exit slit widths to be twice as wide with twice
the radiant flux throughput as for a single monochromator with
the same spectral bandpass. In addition, the magnitude of
stray light rejection is squared for the double monochromator.
For example, if the stray light level for a single monochromator
is 10^{-3} of the input radiant flux, then a double monochromator
of the same design should have a stray light level of 10^{-6} of
the same input radiant flux. The entrance and exit slits are
25 mm tall and 1. 5 mm wide and produce a 10 $\overset{o}{A}$ nominal
spectral bandwidth.

The BUV monochromator uses no fore-optics thus its FOV is the
11. 5° square angular acceptance of the F/5 monochromator.

A calcite Lyot type depolarizer is used to minimize the sensitivity
of the instrument to the polarization state of the backscattered
ultraviolet radiation.   The fundamental differences between the
HROM spectrometer and the BUV spectrometer are these:

1. The HROM spectrometer will use permanently fixed
    gratings and the full spectral image surface from 2500 $\overset{o}{A}$
    to 3400 $\overset{o}{A}$ for the full slit height will be scanned by a
    Hadamard mask.

2. An objective lens is required in front of the entrance slit
    to image a 104° FOV on the 20 mm entrance slit height
    and a 7° FOV on the 10 $\overset{o}{A}$ equivalent entrance slit width.

3. The astigmatic spectral image surface for defining image
    details along the entrance slit height is located about
    10 mm beyond the best astigmatic spectral image surface
    for the Hadamard mask use. This astigmatic entrance
    slit height imaging surface is divided into 15 equal zones

which add up to equal the full height of the entrance slit image. Each of these 15 zones had a width which encompasses all the spectral radiant flux passing through the full 2500 $\overset{o}{A}$ to 3400 $\overset{o}{A}$ spectral image width, 10 mm in front of it. The spectral radiant flux which passes through each of the 15 zones is then conducted to a separate photomultiplier cathode.

6.2.1   Monochromator

The HROM monochromator has an optical layout similar to the SBUV with mirror transfer optics. The three-mirror transfer system has the advantage of not causing monochromator defocusing as a function of wavelength. One mirror is mounted singly while the other two mirrors form a roof mirror system with two precision prisms mounted together. This type of block construction should enable the roof mirrors to be fabricated very accurately, and then to be mounted together accurately and securely. This block approach also minimizes the volume required for mounting. While the gratings for the SBUV Subsystem monochromator will be made from a different master and will probably have a different ghost pattern, the SBUV slit transfer function should be very similar to that of the BUV instrument for most wavelengths over the 1600 $\overset{o}{A}$ to 4000 $\overset{o}{A}$ wavelength range. The slit transfer function of the SBUV may be slightly different near 1600 $\overset{o}{A}$ or 4000 $\overset{o}{A}$ due to slit curvature effects. If 2400 1/mm fixed gratings are used the spectral image width is 2 inches at the intermediate slit and 4 inches at the exit slit. This means the monochromator entrance/exit slit center line, and intermediate slit center line must be 4 inches further apart than on the BUV, and the 15 photomultipliers must receive spectral

radiant flux from a 4-inch spectral image width.

1200 l/mm gratings reduce these spectral image widths by half.
600 l/mm gratings quarter them, so the intermediate slit spectral
image width is 1/2 inch while the exit slit spectral image is
1 inch. The monochromator which has been layed out for this
study uses 600 l/mm gratings which gives a nearly square
spectral image with a spectral image width of roughly 20 mm and
a height equivalent to the entrance slit height of 20 mm. The ray
traces for the monochromator are shown in Figures 6.3, 6.4 and
6.5.

The spacing between the entrance/exit slit center line and the
intermediate slit center line must be increased about 25 mm.

The excellent stray light rejection capability of the BUV instru-
ment implies that the HROM stray light rejection capability should
be excellent, since the same stray light control techniques will
be used. This should allow accurate photometric measurements
of weak spectral regions in the presence of strong solar
emission lines or continuum. The response of the BUV instrument
looking at the zenith sky from ground level is shown in Figure 6.6.
The stray light level at wavelengths below 2800 $\overset{\text{o}}{\text{A}}$ is six decades
below the solar continuum at 3200 $\overset{\text{o}}{\text{A}}$. The intensity falloff which
occurs between 3200 $\overset{\text{o}}{\text{A}}$ and 3400 $\overset{\text{o}}{\text{A}}$ is due to the reflective
attenuation by the coating on the collimating mirrors.

The possibility that stray light due to multiple diffraction by the
grating may pass out through the exit slit of the HROM mono-
chromator was studied. The result of this study once again
confirms that all wavelengths which are multiple-diffracted by
the first grating either go out the entrance slit or impinge upon
the monochromator walls on the entrance slit side of the

HROM--DOUBLE EBERT--F/S--250MM FL-2400 L/MM GRATING--TRI-MIRROR   1600 A   5-7-73
X:Z   0.03937 :1
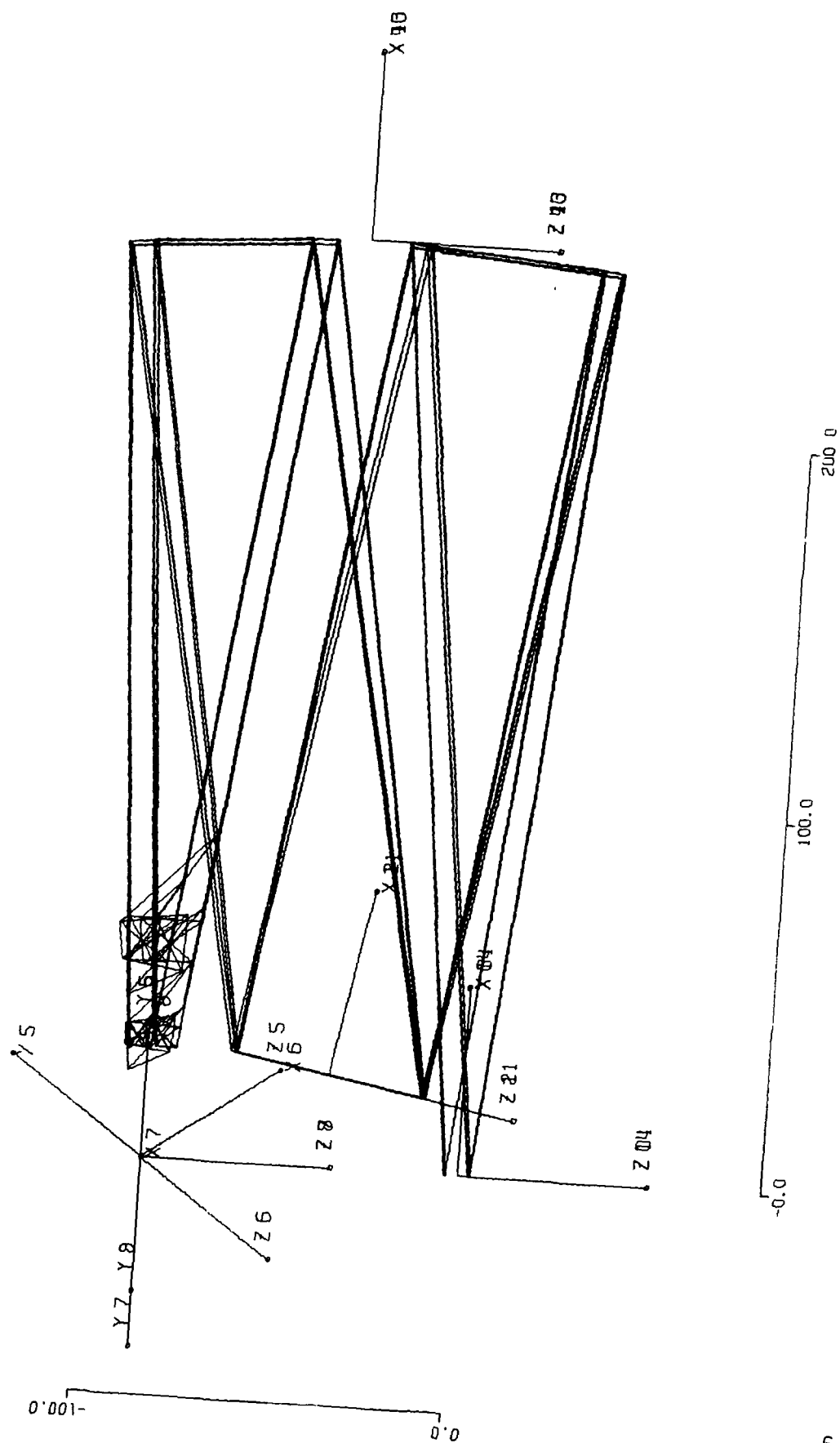
Figure 6.3

HROM-DOUBLE EBERT-F/S-250MM FL-2400 L/MM GRATING--TRI-MIRROR   1600 A   5-7-73

X:Y   0.03937 :1
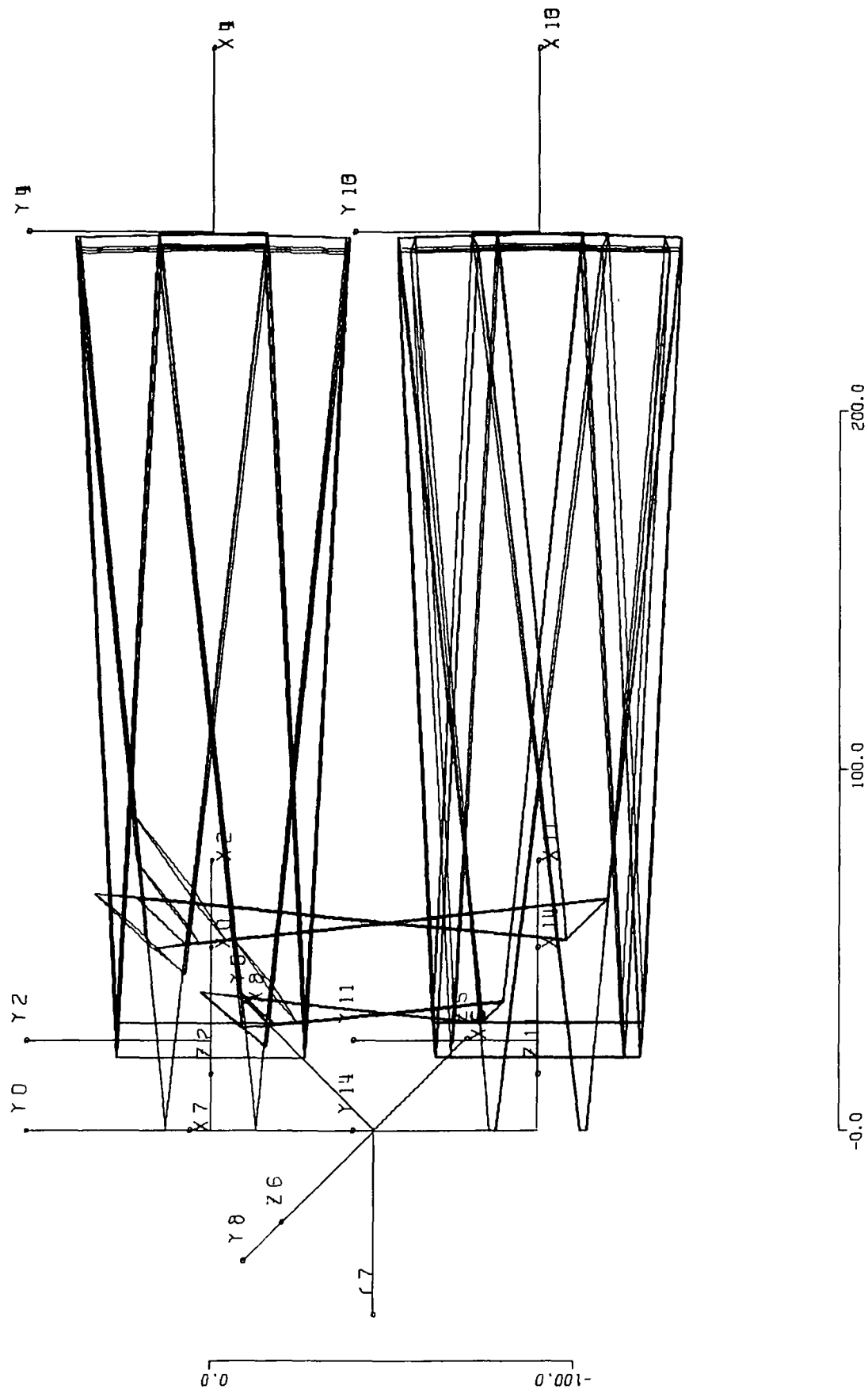
Figure 6.4

HROM·DOUBLE EBERT-F/S-250MM FL-2400 L/MM GRATING--TRI-MIRROR· 1600 A · 5-7-73
Z:Y   0.03937 :1

Figure 6.5

6 - 9
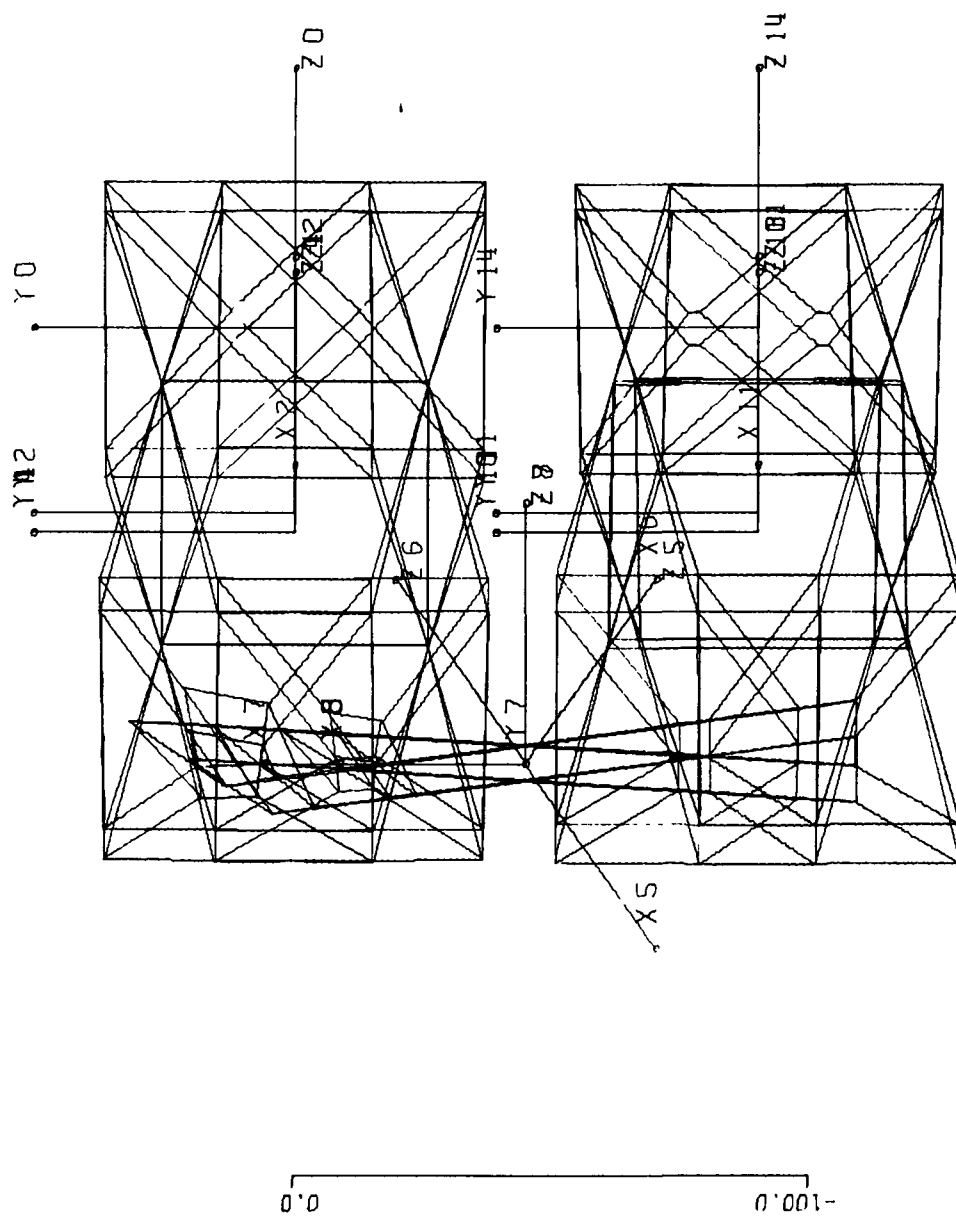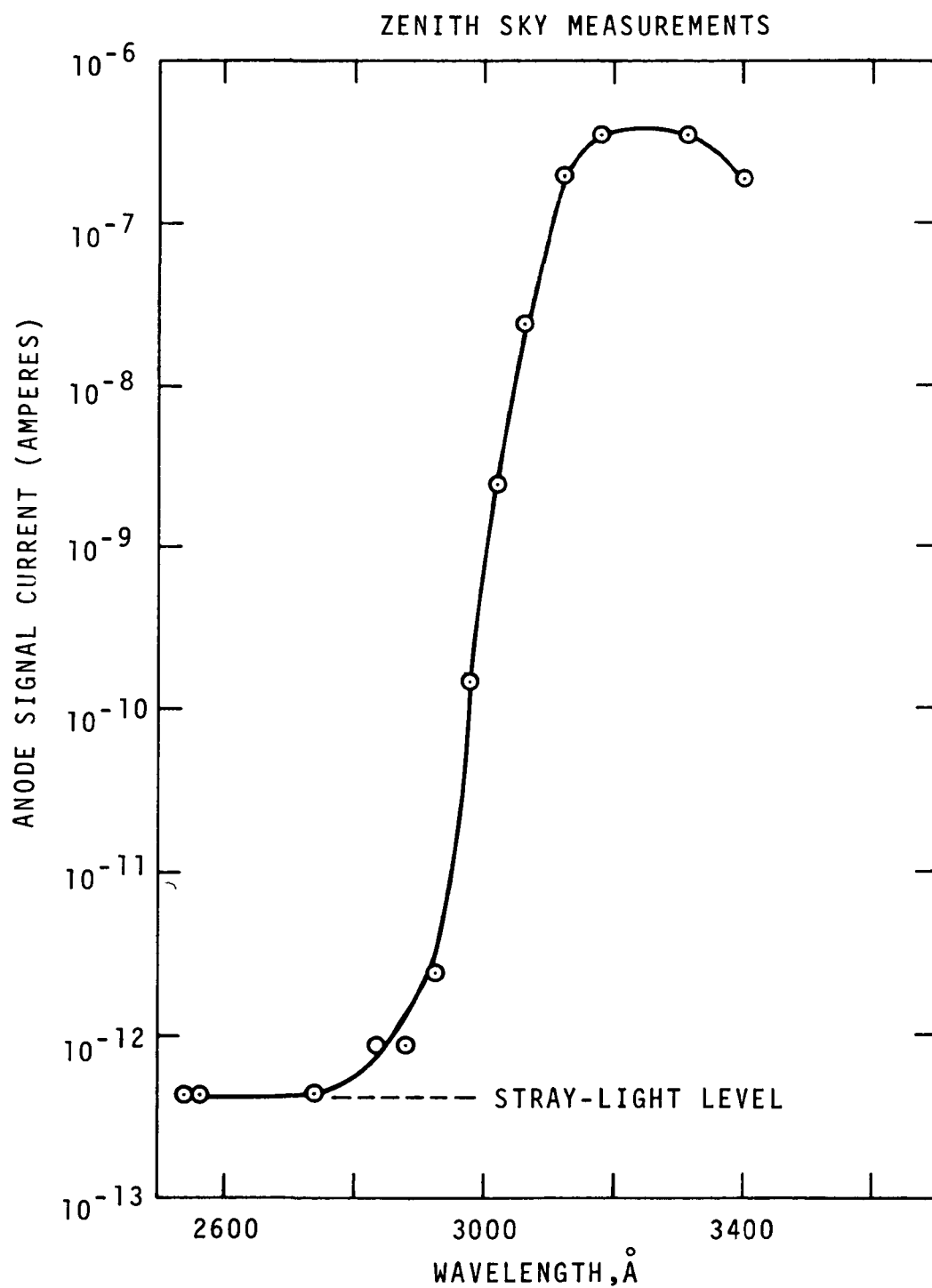
Fig. 6.6 Response of the BUV Instrument looking at the Zenith Sky from ground level.

monochromator.

6.2.2 Objective Lens

The objective lens must have a short focal length to produce a 52° half angular FOV at the upper or lower ends of the 20 mm tall entrance slit. This lens is used at only F/5 but it must have a very large diameter to properly focus the monochromator acceptance rays for the full 20 mm tall entrance slit.

Fused silica has too low an index of refraction to be used for the positive element of this lens, thus sapphire is used.

For an inline objective lens system, the 104° FOV, unfortunately, is vignetted by the photomultiple mounting system, therefore, the entrance optics have been rotated 90° by a fused silica prism. The prism surfaces have been given negative correction to reduce chromatic aberrations.

6.2.3 Detector Optics

The assembly drawing Figure 6.2, shows an arrangement of 15 photomultiplier tubes relative to the spectral image surface. Fifteen identical fused silica plates are used to conduct the spectral radiant flux from the 15 zones of the spectral image to separate photomultipliers.

These plates are each 1.33 mm thick, and plane parallel in a side view. Seen in a plan view, they are slightly trapazoidal tapering from a 20 mm width at the spectral image surface to an 8 mm width at the photomultiplier.

6.3 Detector Module

The HROM has been designed to use the EMR Type 510 photomultipliers, which is physically much smaller than the photomultipliers previously used in the BUV and SBUV systems. The EMR Type 510N-06-07 photomultiplier uses a bi-alkali photo-

cathode and a suprasil window. While these photomultipliers may be considered somewhat developmental they should have flight experience in time to be used for the HROM program.

The HROM uses the type N bi-alkali photocathode which has a high (20% typical, not including window) and flat quantum efficiency at wavelengths less than 4000 $\overset{O}{A}$.

6.3.1   Window Selection

The PMTs use fused silica as a window material. This material was chosen because it exhibits much less scintillation emission in the presence of Bremsstrahlung photons resulting from high-energy electrons. Experience with the NIMBUS-4 BUV, which employed two PMTs with sapphire windows, indicates that scintillation-produced background would interfere with the minimum signals to be processed by the HROM if sapphire windows were used. EMR PMTs are made in a modular manner, with dynode elements in the form of circular stamped plates separated by glass rings. PMTs are potted with dynode divider resistors in place. The dynode resistors are metal glaze types.

6.4   Mechanical Design

In this design, all optical elements are stationary except for the diffuser assembly and the rotating Hadamard Mask. A layout drawing of the instrument is shown in Figure 6.2.

6.4.1   Mechanical Configuration

The monochromator is constructed in a monolithic housing. Cast from A356 aluminum alloy, the housing is precision machined and provides direct mounting of all optical elements on lapped

integral seats. The detector and diffuser assemblies also mount directly on the housing. This direct mounting technique minimizes assembly time and assures position and alignment stability of all optical elements. To minimize the effects of thermal defocusing and thermal gradients within the telescope, the reflective elements are mono-metallic with the housing (all are aluminum). The differential thermal coefficient between the A356 alloy housing and the 6061 alloy mirrors is only 1 microinch per inch per degree F. Using aluminum mirrors maintains the geometrical relationships of the optics with the housings over a broad temperature range. This approach eliminates the need for an expensive structure to provide low thermal expansion and instead provides a high thermal diffusivity to prevent the occurrence of thermal gradients. Aluminum mirrors also reduce weight and simplify mirror mounting techniques.

The system can be thermally controlled by passive techniques and thermally isolated from the Spacecraft mounting structure. The instrument utilizes a multi-layer aluminized mylar insulation blanket to minimize orbital thermal variations. An internal heater and a nadir-facing radiator may be included to accommodate various potential duty cycles and power dissipations. These techniques can maintain the instrument within a 10°C temperature range and provide instrument temperature stabilities in the order of 0.5°C.

The instrument is designed for a single-plane mount with the s/c. The weight of the proposed design is 15 kg and the volume is 0.305 m high by 0.305 m wide by 0.61 m high.

The collimating mirrors and grating substrates are made of 0. 2 inch thick, nickel plated, stabilized 6061-T6 aluminum. A rib pattern is added to the rear of the mirrors to facilitate fabrication to the required figure of one-fourth wave.

The fundamental reasons for the use of the metal optics is to overcome tilt, de-center and defocusing errors as a result of differential thermal expansion between the optical parts and their housings. Metal optics are particularly suitable for optical systems which must withstand severe temperature changes and yet remain in alignment.

6. 4. 2   Diffuser Plate Mechanism

The diffuser plate is a transmissive element similar to the design employed on the BUV instrument flown on Explorer 55.

The diffuser plate mechanism must deploy the diffuser plate into the field-of-view on command. It must also provide protected storage to prevent surface degradation due to long-term exposure.

The diffuser plate is driven by a permanent magnet stepper-gearhead combination, and the entire mechanism is a removable assembly.

Verification of diffuser plate position is accomplished with LED-photodiode pairs. Only two positions need be sensed-- stowed and calibrate, so a simple pattern of small holes in the gear web will suffice. The rotating output member is balanced, so that motor detent torque multiplied by the gear ratio is sufficient to hold the output against rotation due to launch vibration.

6.4.3   Hadamard Mask Drive Mechanism

The Hadamard disc will be a 10 inch diameter thin (0.001 inch)
metal plate. It will be stepped in 16 equally spaced angular
positions holding in each position approximately 400 milliseconds
and stepping to the next position in 10 milliseconds. The step
will be accomplished by means of a small constant speed DC
motor dissipating 2 watts. The motor will drive a momentum
storing wheel (a flywheel) which will have an escapement
mechanism drawing power from the stored energy at the proper
intervals.

Since the energy required to accelerate/decelerate the Hadamard
disc is only a fraction of a watt, the mechanical efficiency of
the escapement need only be better than a few percent, which
is easily obtainable.

6.5   Electronic System

6.5.1   Signal Processing Electronics

A block diagram of the signal processing electronics is shown
in Figure 6.7. The system employs 15 electrometer preamplifiers,
one for each UV detector. The output of each detector is inte-
grated for the mask dwell time (a little under 400 milliseconds)
and converted to a 12 bit digital code. This is compatible with
the required 1% radiometric precision as shown in Appendix B.
If the output of the integrator at any code position exceeds 87.5%
of the full scale value of the ADC, a flag is set which is used to
reduce the gain of the preamplifiers at the completion of the mask
cycle. Conversely, if the output of the integrators at any mask
position other than the opaque position fails to exceed 25% of
the full scale value of the ADC, a flag is set which is used to
increase the gain of the preamplifiers at the completion of the
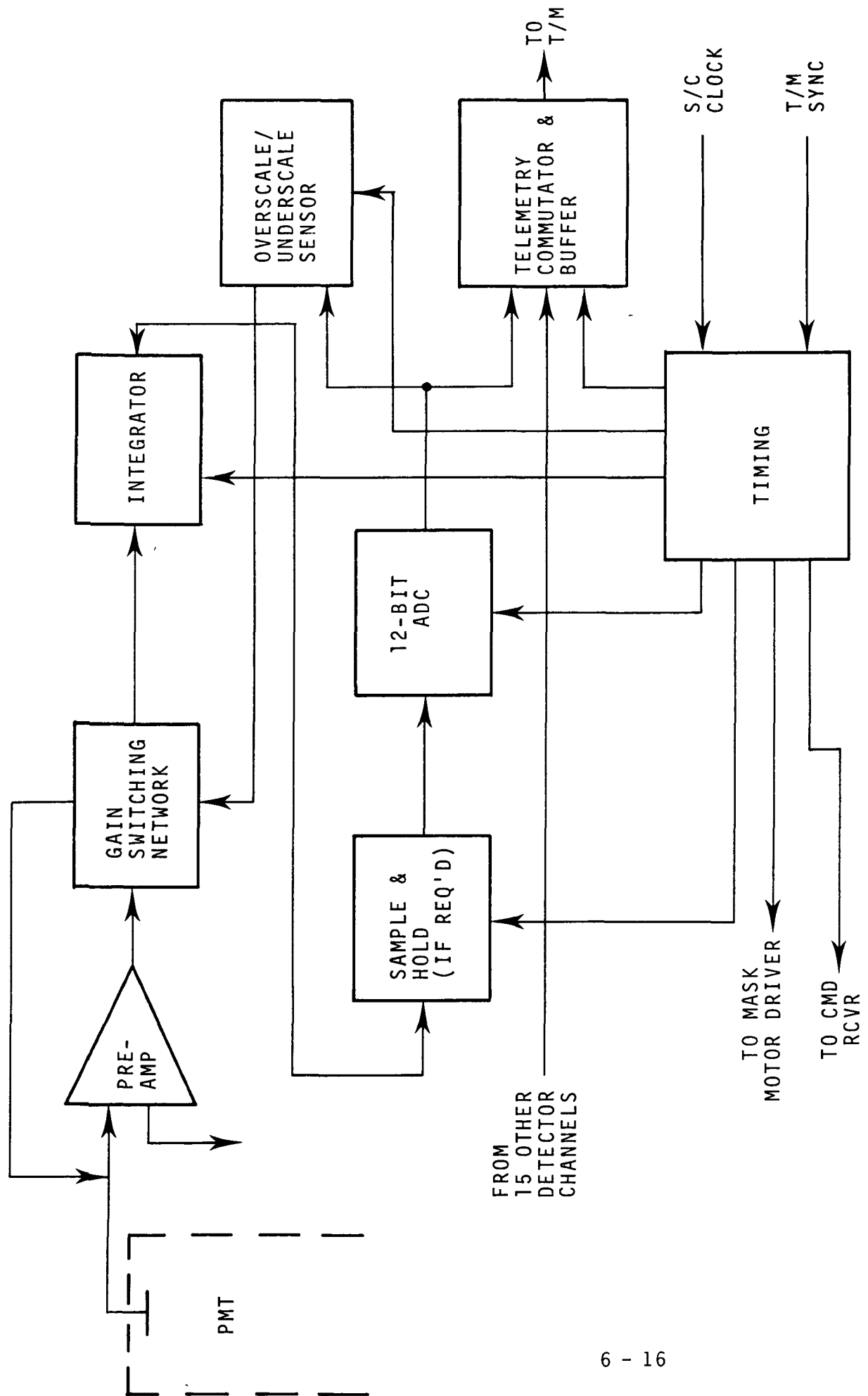
Fig. 6-7 Signal Processing Electronics Block Diagram

mask cycle. One mask cycle is completed in 7.38 seconds, the time required for the scene viewed by the spectrometer to advance by one resolution element. During this mask cycle, 240 measurements are obtained, one for each detector for each of the 16 mask positions.

One of the mask positions is completely opaque. It thus yields a black level calibration for the system and also provides verification of proper tracking between the mask cycle and the telemetry main frame timing.

Because of the long duration of the measurement cycle, the possibility of commutating a single ADC among the 15 signal channels could be entertained. It seems, however, that with the advent of inexpensive microcircuit converters the resulting savings in hardware would be minimal, and would be more than offset by loss of the redundancy inherent in the use of independent parallel data channels.

6.5.2   Hadamard Mask Driver

The Hadamard Mask Driver advances the mask by one position after the integration of each sample. The time interval while the mask is in motion is not available for signal integration, and should therefore be minimized. The required cycle time for each mask position is a little less than 400 milliseconds. This is based on the spatial and spectral resolution requirements of the instrument. An advance time of 10 milliseconds would correspond to an equivalent collection efficiency of 98% and would therefore seem acceptable.

To achieve such rapid motion with an acceptable power level, a low inertia system is required. The present primary candidate

system is a thin disk driven by a DC motor with a flywheel. Aside from the Hadamark Code slits, the disk contains a code pattern suitable for detecting and identifying sixteen positions by means of an electro-optical sensor.

In normal operation, the disk is driven from each position until the next position is detected. One of the sixteen positions, corresponding to a fully opaque mask, is identified as the home position. At this position, a tracking counter is reset which is advanced each time the disk is advanced. The state of the counter is subsequently compared to the position indicator and sets an alarm flag if disk position and tracking counter indication ever fail to agree. This alarm flag is transmitted to the ground by way of telemetry to alert the data reduction team that the corresponding measurements are suspect.

A Back-Up Operating mode, used in case of failure of the position sensing system, advances the code disk by a predetermined number of stepper motor steps to the next position. Ground-commanded single step capability allows proper phasing of the wheel in this mode.

6.5.3   Calibration

Spectral and intensity calibration cycles are provided.

Spectral calibration is accomplished by a suitable spectral lamp illuminating the entrance aperture of the instrument. The electronic system provides power to start and operate the spectral lamp at the required intensity.

Intensity calibration is accomplished by inserting a sunlit diffuser in front of the mapper's entrance slit. The electronic system provides the electrical driving signal to actuate a suitable

mechanism. Electrical timing signals control power for the spectral lamp and for the diffuser mechanism in such a manner that a calibration cycle starts and terminates at the opaque position of the Hadamard mask. The calibration cycles are thereby constrained to last an integral number of full cycles. This minimizes lost data and facilitates data reduction. Calibration cycles are identified by a suitable flag in the housekeeping data bit stream.

Black level calibration is obtained once each Hadamard cycle, by letting one position of the mask disk be fully opaque.

6.5.4   Housekeeping and Diagnostics

The HROM provides housekeeping data to assist data reduction. This data will include commutated binary digital signals as well as uncommutated analog signals. Digital signals include:

> An indication that the mask wheel is tracking.
>
> An indication that the amplitude cal lamp is on.
>
> An indication that the amplitude cal diffuser is in.
>
> An indication of the gain state of each detector channel.
>
> An indication of the operating modes of the instrument selected by command.

Analog signals include:

> Indications of the following four temperatures:
>
>> Detector Assembly
>>
>> Code Disk Drive Motor
>>
>> Electronics Assembly
>>
>> Low Voltage Power Supply
>
> An indication of the several output voltages of the low voltage power supply.
>
> An indication of the output voltage of each high voltage power supply.

Digital housekeeping signals are obtained by sensors directly monitoring the condition of interest, or by sensing the power actually supplied to the actuator or exciter.

Temperatures are measured by miniature thermistors fastened to the assembly or part to be monitored by means of a thermally conductive bonding material. The conductance of the thermistors is measured by conditioning circuits with a calibrated transfer characteristic. Suitable buffering is provided to prevent loading.

Voltages are monitored by divider networks. When negative voltages are monitored, an operation amplifier provides inversion for telemetry compatibility.

6.5.5   Commands

The HROM contains provisions for receiving serial command data from the spacecraft command system. The instrument command circuitry comprises a command receiver, decoders, and control registers. The receiver accepts command data from the space-craft interface in serial form and provides a parallel output that is valid immediately after command data is received. The decoders route the appropriate command data to the proper control register and the control registers accept and store the command data and use it to control the operational deployment of the instrument. Control registers are generally updated at the end of a Hadamard code cycle so that instrument configuration is changed at the opaque position of the mask.

Commands are used, among other functions, for the following purposes:

> To activate or deactivate the spectral calibration source

> To activate or deactivate the intensity calibration diffuser

To switch the mask disk drive from the manual mode to the back-up mode or vice-versa

To enable or disable any one or more high voltage power supplies

To advance the code disk by a single motor step in the back-up mode of operation

If compatible with the spacecraft command system, commands will be encoded in such a manner that each of these functions can be controlled independently of the others without reference to the prior command configuration of the spectrometer.

APPENDIX A

Theory of Hadamard Spectrometers

A - 1 Codes For Hadamard Transform Spectrometry

Now consider a Hadamard-transform spectrometer which is encoded only in the exit focal plane.

Let W be an NxM matrix whose rows represent the M encoding masks successively placed in the exit plane of such a spectrometer. A very desirable characteristic of W is that it be cyclic; that is, the $(i+1)^{st}$ row of W is obtained by shifting the ith row cylically one place to the right.

Such a mask has two advantages. First, it can be self-supporting and therefore permits the construction of a spectrometer which requires no transmission materials. In operation, the mask is stepped one slit width along the length of the mask- i.e., in the direction of dispersion - for each successive encoding position.

More important, perhaps, cyclic codes enable us to avoid the tedious construction of N masks each having N slots, for a total of N^2 slots. Instead we construct only one mask with 2N-1 slots. The cost of mask construction is reduced by $\sim\frac{1}{2} N$ and the design of the advance mechanism is considerably simplified since the bulk weight of the masks also decreases as $\sim\frac{1}{2}N$.

Singly-Encoded Instruments

Sloane, et. al. (1969) have developed the following theory:
The optical spectrum whose shape is to be estimated is
spatially dispersed and the band of interest partitioned into
N channels.   The average energy in the jth channel, after a
selected integration time, is denoted by ψ_j. The measurement
process consists of observing the spectrum through M masks,
the energy through the ith mask being $\sum_{j=1}^{N} \omega_{ij} \psi_j$ where W_i =
$(\omega_{i1}, \ldots, \omega_{iN})$ is the ith vector of mask elements.   The
photodetector adds a random noise v_i to the signal $\sum_{j=1}^{N} \omega_{ij} \psi_j$
and yields a measurement

$$\eta_i = v_i + \sum_{j=1}^{N} \omega_{ij} \psi_j, \quad i = 1, 2, \ldots, M. \qquad (A-1)$$

The noise v_i has the following properties: $\langle v_i \rangle = 0$; v_i is
independent of the signal: $\langle v_i^2 \rangle = \sigma^2$; successive measurement
noises are assumed to be uncorrelated ($\langle v_i v_j \rangle = 0$ if $i \neq j$) and
$\langle \ \rangle$ represents an ensemble average.

In order to extimate $\{\psi_j\}$ by $\{\hat{\psi}_j\}$ we need at least as many
measurements M as there are unknowns N. Furthermore, at
least N distinct masks $\{W_i\}$ are needed to estimate the spectral
shape.   Hence, assume vectors of observations $\underline{\eta} = (\eta_1, \ldots, \eta_M)$,
channel energies $\underline{\psi} = (\psi_1, \ldots, \psi_N)$, measurement noises $\underline{v} =$
$(v_1, \ldots, v_M)$, and a matrix of masks W $= (W_1^T, \ldots, W_M^T) =$
(ω_{ji}). $\Big($The T stands for transpose$\Big)$. With this notation $\underline{\eta} = \underline{\psi}W + \underline{v}$.
An estimate of $\underline{\hat{\psi}}$ of ψ is a function of the observations, ψ (η),
expected to lie close to $\underline{\psi}$. As a measure of the accuracy of the

estimate we adopt the mean square error criterion: We minimize
$\epsilon = \langle (\hat{\underline{\Psi}} - \underline{\Psi})(\hat{\underline{\Psi}} - \underline{\Psi})^T \rangle$.

For purposes of computational convenience we agree to restrict $\hat{\underline{\Psi}}$ to be a linear function of the observations, $\hat{\underline{\Psi}} = \underline{\eta}A$, for some matrix A; in the absence of more detailed statistical knowledge concerning the anticipated spectral shape or the photodetector noise characteristics, this seems appropriate. Before an essentially uniquely best experimental design can be derived, however, we still need to make the assumption that the estimator is unbiased; i. e. $,\langle \hat{\underline{\Psi}} \rangle = \underline{\Psi}$. This assumption can be defended on the following grounds: 1) we need an estimator which, on the average for a large number of applications, yields the true value; 2) the unbiased estimator can be shown to be desirable when there is a large uncertainty in $\underline{\Psi}$ relative to our prior knowledge of the spectrum and the measurement noise power.

We must now select those matrices A, W that minimize ϵ subject to the constraint we have set. First we see that

$$\langle \hat{\underline{\Psi}} \rangle = \langle \underline{\eta} A \rangle = \langle \underline{\eta} \rangle A. \qquad (A-2)$$

Furthermore,

$$\langle \underline{\eta} \rangle = \langle \underline{\Psi} \rangle W + \langle \underline{\nu} \rangle = \langle \underline{\Psi} \rangle W. \qquad (A-3)$$

Hence, unbiasedness requires that WA = I, the identity matrix. If M = N, W is square, and $A = W^{-1}$. If W is not square but is N x M (M > N), we can use the generalized inverse.

$$A = W^T(WW^T)^{-1}. \qquad (A-4)$$

Having solved for A in terms of W we now select W to minimize $\epsilon = \langle (\hat{\underline{\Psi}} - \underline{\Psi})(\hat{\underline{\Psi}} - \underline{\Psi})^T \rangle$. We note that

$$\hat{\Psi} - \Psi = \Psi WA + \nu A - \Psi = \nu W^T(WW^T)^{-1}. \tag{A-5}$$

By assumption $\langle \nu^T \nu \rangle = \sigma^2 I$. Thus

$$\epsilon/\sigma^2 = \text{Trace } [W^T(WW^T)^{-1}(WW^T)^{-1}W]. \tag{A-6}$$

If $M = N$, this simplifies to $\epsilon/\sigma^2 = \text{Trace } (W^{-1}(W^{-1})^T)$. The optimum experimental design will be completed if we can find that W – subject to $\omega_{ij} = 0$ or 1 or -1 – that has the minimum ϵ/σ^2.

A – 3   Choice of Masks

We just showed that in the case $M = N$, when there are as many measurements as unknowns, the matrix $W = (\omega_{ij})$ of mask elements should be chosen so that for $\omega_{ij} = 0$ or 1 or -1, $\text{Tr } (W^{-1}(W^{-1})^T)$ is as small as possible. Three possible choices for the matrix W are given here. See Appendix A of Sloane et. al. (1969) for the characteristics of Hadamard matrices needed to understand the following results:

If H is an $N \times M$ normalized Hadamard matrix, and G is in the $(N - 1) \times (M - 1)$ matrix obtained by deleting the first row and column of H, and S is obtained from G by replacing $+1$'s by 0's and -1's by $+1$'s then three possible choices for the matrix W of mask weights, together with the corresponding values of $\text{Tr } (W^{-1}(W^{-1})^T)$, are as follows: (Table A – 1)

We may note that

(a)   Another choice for W is R^T, where R is the matrix obtained from G by replacing -1's by 0's. This gives a trace, however, which is slightly but uniformly worse than that from S^T.

(b)   All the matrices given in Table A-1 are superior to the single slit case (where $W = I$). In the single slit case Trace $= N$.

TABLE A - 1

Mask Weights

Matrix W	Trace	Elements
H^T	1	+1, -1
G^T	2-2/N	+1, -1
S^T	$4-8/N+4/N^2$	+1, 0

(c) Nelson and Fredman (1970) , Philips (1972) , and
Sloane and Harwit (1976) have shown that the Hadamard
matrix and its variations describe a set of optimum masks.

A - 4 <u>Optical Arrangement</u>

A multislit spectrometer using the S^T code works as follows:
Radiation which passes through the entrance aperture is
rendered parallel and directed towards the dispersive element.
The dispersed radiation is collimated and focuses upon the multi-
slit mask at the exit plane of the instrument.

The radiation transmitted by the mask passes through the post-
optics of the system and impinges on the detector. We then
obtain a spectrum by sequentially stepping M masks at the exit
plane and recording the detector output for each mask. The
inversion procedure described above then enables us to recover
the spectrum.

In some instances, depending upon instrumental design and the
choice of code, it may be advantageous to make use of both the
reflected and transmitted radiation of a mask. This scheme
would be particularly useful for masks which utilize the H^T and
G^T matrices. Here the + 1's would represent reflecting slots
and the - 1's would represent transmitting slots. For the H^T
matrix all elements of the first column would be + 1's and the
masks corresponding to each row of H^T would reflect the first
spectral element at all times. The remaining N -1 slots would
be stepped in the usual fashion. Such instruments have not yet
been constructed.

Infrared spectral measurements normally require that the radiation
be chopped. One can then realize codes with 0's and 1's by
chopping between the transmitted radiation and a standard

source. The codes with + 1's and - 1's could be realized by chopping between transmitted and reflected radiation.

A - 5 Comparisons with Other Dispersive Spectrometers

To make a fair comparison, we assume: (1) a fixed total measuring time T; (2) constant slit widths; and (3) an equal number N of unknown spectral elements to be estimated. For the doubly encoded system there are initially $2N - 1$ unknowns $\Psi_{-(N-1)}, \cdots, \Psi_0, \cdots, \Psi_{N-1}$, but for this comparison we will suppose we only wish to estimate the N central elements

$$\Psi_{(N-1)/2}, \ldots, \psi_0, \ldots, \Psi_{(N-1)/2}$$

(taking N odd for convenience). Of course, we can still obtain some estimate of the ends, but these errors will not appear in the comparisons.

As a measure of performance we take, as before, the total mean square error in all the unknowns:

$$\sigma^2_{total} = \sum_{t=-(N+1)/2}^{(N+1)/2} \sigma^2_t \tag{A - 7}$$

Table A-2 compares three different grating spectrometers. The first column is for a single entrance and exit slot. N measurements are made in time T, with a mean square error σ^2 in each, and the second column is for a singly multiplexed instrument with an exit mask.

A - 7

TABLE A-2

Comparison of total mean square error for two grating spectro-
meters in estimating N unknowns

N	Conventional	Singly Encoded
3	$3\sigma^2$	$2.25\sigma^2$
7	$7\sigma^2$	$3.06\sigma^2$
11	$11\sigma^2$	$3.36\sigma^2$
19	$19\sigma^2$	$3.61\sigma^2$
N	$N\sigma^2$	$\{2 - 2/(N + 1)\}^2\sigma^2$

(σ^2 is the mean square noise in a single measurement made in
time T/N; σ^2 = (constant) N/T).

Dynamic Range Requirements for High Resolution Ozone Mapper

Statement of the Problem:

It is desired to calculate the dynamic range required to transmit the Hadamard coded signal of the High Resolution Ozone Mapper without significant degradation due to the noise (or digitization level) of the transmission channel. The High Resolution Ozone Mapper is a 16 – channel spectrometer. Twelve spectral data channels are coded by Hadamard techniques.

Discussion:

The proposed instrument achieves the 12 elements of spectral information by 16 code mask positions. Hence the analysis for a 16 element instrument is appropriate. We therefore assume

$n = 16$ spectral elements
$n = 16$ mask positions (i.e., 1 Hadamard sample = 1 signal
         measurement per mask position)
$n = 16$ time elements
   N Photons incident, total spectrum, total scan

During each time element, N/n photons are incident on the instrument and, since $n/2$ mask elements are opaque, on the average the detector sees $N/2n$ photons, N/n^2 from each transparent mask element.

The incremental signal for one spectral element, i.e., the amount by which the signal from that element deviates from the average, is computed by subtracting the sum of the signals for the $n/2$ mask positions for which that spectral element is opaque from the sum of the signals for the $n/2$ mask positions for which the same spectral element is exposed.

If this computed signal ($\Delta\Phi$, expressed as a number of photons detected) is generated by an actual differential in photons (ΔN) associated with that spectral element, then $\Delta\Phi$ and ΔN are related by

$$\Delta\Phi = \frac{n}{2} \text{ mask positions } \times \left(\frac{N}{2n} + \frac{\Delta N}{n}\right) \text{ photons } -$$

$$\frac{n}{2} \text{ mask positions } \times \frac{N}{2n} \text{ photons } = \frac{\Delta N}{2} \text{ photons}$$

The noise or uncertainty in the measurement is then obtained as the quadrature sum of the noise associated with each time element. The noise for each of the $n/2$ elements for which the spectral element is exposed is

$$E_e = \sqrt{\frac{N}{2n} + \frac{\Delta N}{n}}$$

and the noise for each of the n/2 elements for which the spectral element is opaque is

$$E_O = \sqrt{\frac{N}{2n}}$$

Hence the total noise is

$$E_T = \sqrt{\frac{1}{2}(N + \Delta N)}$$

For the spectral element of interest, the total signal is given by adding the incremental signal $\Delta \Phi = \Delta N/2$ to the average signal (per spectral element) $N/2n$.

The noise in this total signal is given by the quadrature sum of the noise components. The noise component for the incremental signal is given by E_T above. The noise component for the average signal is $\sqrt{N/2}$, of which $1/n\sqrt{N/2}$ is associated with each spectral element. The signal-to-noise ratio for each spectral element is then given by

$$SNR_\lambda = \frac{1}{2}\left(\frac{N}{n} + \Delta N\right) \div \sqrt{\frac{1}{2}(N + \Delta N) + \frac{N}{2n^2}}$$

and if $n \gg 1$ and $N \gg \Delta N$ this reduces to:

$$SNR_\lambda = \sqrt{\frac{N}{2}}\left(\frac{1}{n} + \frac{\Delta N}{N}\right)$$

If we now add the effects of the noise (ε) associated with the transmission of each Hadamard sample, the total noise (E_T') becomes

$$E_T' = \sqrt{\frac{1}{2}(N + \Delta N + 2n\varepsilon^2)}$$

and a noise $1/n\sqrt{N/2 + n\varepsilon^2}$ is associated with the average signal for each spectral element. The total signal-to-noise ratio for each spectral element is then given by

$$SNR_\lambda' = \frac{1}{2}\left(\frac{N}{n} + \Delta N\right) \div \sqrt{\frac{1}{2}\left(N + \Delta N + 2n\varepsilon^2\right) + \left(\frac{N}{2n^2} + \frac{\varepsilon}{n}\right)}$$

and if $n \gg 1$, $N \gg \Delta N$

$$SNR_\lambda' = \frac{1}{2}\left(\frac{N}{n} + \Delta N\right) \div \sqrt{\frac{N}{2} + n\varepsilon^2}$$

and hence

$$\varepsilon^2 = \frac{1}{n}\left[\left(\frac{N/n + \Delta N}{2\,SNR_\lambda'}\right)^2 - \frac{N}{2}\right]$$

but the highest signal (S) for one interval is

$$S = \frac{N}{2n} + \frac{\Delta N}{n}$$

and if $N \gg \Delta N$

$$S = \frac{N}{2n}$$

and

$$\varepsilon^2 = \frac{1}{n} \left(\frac{2S + \Delta N}{2\,SNR_\lambda{'}} \right)^2 - S$$

then

$$\frac{\varepsilon}{S} = \sqrt{\frac{1}{n} \left(\frac{1 + \dfrac{N}{2S}}{SNR_\lambda{'}} \right)^2 - \frac{1}{S}}$$

therefore if $n = 16$, $SNR \geq 100$, $\Delta N \ll 2S$

$$\lim_{s \to \infty} \frac{\varepsilon}{S} \leq \frac{1}{100} \sqrt{\frac{1}{16}} = \frac{1}{400}$$

or, in words, a transmission channel signal-to-noise ratio of $400 \div 1$ is required for a radiometric accuracy of 1%. It can also be seen that the required signal-to-noise ratio is reduced when ΔN is not small compared to 2S, i.e., when the energy is not equally distributed among spectral elements. It can therefore be concluded that the required $400 \div 1$ signal-to-noise ratio refers to a worst case situation.

It should be noted that this signal-to-noise ratio is required if one measures the transform signal with respect to the dark level, and therefore the range of the encoder must extend from the dark level to the signal level. In several applications the required dynamic range does not extend down to the dark level. In an instrument that uses Hadamard techniques to code image data, for example, all samples remain fairly close to the average. Unfortunately, that is not so in a spectrometer, since the full range of signal levels is required to encode a spectrum that consists entirely of one strong emission line.

REFERENCES

1. Fellgett, P. (1951). Doctoral Thesis, Cambridge University.

2. Fellgett, P. (1958). J. Phys. Radium 19, 187

3. Decker, J. A., Jr. (1974a). In "Applications of Walsh Functions and Sequency Theory" (H. Schreiber and G. F. Sandy, eds.), pp. 229-248. IEEE, New York.

4. Tai, M. H., and Harwit, M. (1976). Private communication.

5. Sloane, N. J. A., Fine, T., Phillips, P. G., and Harwit, M. (1969). Appl. Opt. 8, 2103.

6. Nelson, E. D., and Fredman, M. L. (1970) J. Opt. Soc. Amer. 60, 1664.

7. Phillips, P. G., (1972). Ph.D. Thesis, Cornell University.

8. Sloane, N. J. A., and Harwit, M. (1976). Appl. Opt. 15, 107.

9. Decker, J. A., Jr. (1971). Appl. Opt. 10. 510.

10. Chester, T. L., Fitzgerald, J. J., and Winefordner, J. D. (1976). Analyt. Chem. 48, 779.

11. Oliver, C. J. (1976). Appl. Opt. 15, 93.

12. Oliver, C. J., and Pike, E. R. (1974). Appl. Opt. 13, 158.

13. Larson, N. M., Crosmun, R., and Talmi, Y. (1974). Appl. Opt. 13, 2662.

14. Pratt, W. K., Kane, J., and Andrews, H. C. (1969). Proc. IEEE 57, 58.

15. Slingerland, J. (1975). Rev. Sci. Instrum. 46, 746.

16. Mertz, L. (1965). "Transformations in Optics." Wiley, New York.

17. Tai, M. H., Harwit, M., and Sloane, N. J. A. (1975b). Appl. Opt. 14, 2678.

REFERENCES (Cont'd)

18.   Griffiths, P. R. (1974). Analyt. Chem. 46, 645A.

19.   Hirschfeld, T. (1976) Analyt. Chem. 48, 721.

SUBJECT INDEX

1

2

SUBJECT INDEX (Continued)

<u>SUBJECT INDEX</u> (Continued)